Chapter 2

MATURE STRUCTURE AND EVOLUTION

H. E. Willoughby

[This chapter draws heavily upon Greg Holland's "Chapter 2, Mature Structure and Structure Change" of *A Global View of Tropical Cyclones* and on the author's (1988) review article "Dynamics of the Tropical Cyclone Core" in the *Australian Meteorological Magazine*. It benefitted greatly from material on air-sea interaction provided by Jeff Kepert of the Bureau of Meteorology Research Centre and from careful review of an earlier draft by colleagues at the Hurricane Research Division: P. G. Black, R. W. Burpee, and John Kaplan.]

2.1 INTRODUCTION

Over much of the tropical oceans in summer, the process of bringing the tropospheric column to thermodynamic equilibrium with the sea would add enough heat to lower the surface pressure by 5-10% (Miller 1958). Although tropical cyclogenesis is emphatically not a simple mixing process, the atmosphere's adjustment of the balance wind and mass on a rotating Earth toward the low pressure attainable at equilibrium is the reason that tropical cyclones exist.

A tropical cyclone (TC) is thus a warm-core vortex. The winds that swirl about the center decrease with height, but typically fill the depth of the troposphere (Haurwitz 1935). This inner region, termed the cyclone "core," contains the spiral bands of precipitation, the eyewall, and the eye that characterize tropical cyclones in radar and satellite imagery (e.g., Wexler 1947; Dvorak 1975). The inner region winds can become intense, and in extreme cases reach 90 m s^{-1} just outside the eye.

The primary circulation--the tangential, or swirling, wind---in the core becomes strongly axisymmetric as the cyclone matures. In addition to the primary circulation, a secondary circulation arises in response to surface friction and condensational heating. As shown in Fig. 2.1, it has radial inflow near the surface, saturated ascent around the eye, forced descent inside the eye, and outflow near tropopause level outside the eye. The inflowing air loses angular momentum to the sea, so that after it rises and turns outward, it swirls anticyclonically about the center beyond 100-200 km radius (Riehl 1963). The secondary circulation supplies the angular momentum and thermal energy that intensify the primary circulation and maintain it against friction and radiative cooling (Riehl and Malkus 1961). In the core, the primary circulation is much stronger than the secondary circulation. Many features in the core persist for days (Malkus *et al.* 1961) -- that is, for tens of rotation periods (~ 1 h) of the air moving around the center with the swirling wind.

As Fig. 2.2 shows for a Southern Hemisphere cyclone, the axisymmetric core is characteristically surrounded by a less symmetric outer vortex that grades into the synoptic environment. In the lower troposphere, the cyclonic circulation may extend more than 1000 km from the center (Frank 1977a). The boundary between cyclonic and anticyclonic circulation slopes inward with height, so that the circulation in the upper troposphere is primarily anticyclonic except near the center. In the outer vortex, there are no scale separations between the primary and the secondary circulations, the asymmetric motions, or the vortex translation. The asymmetric flows in this region control the vortex motion and sustain an eddy convergence of angular momentum into the center (Pfeffer 1958). One prominent asymmetry arises from advection of planetary vorticity from high to low latitudes by the swirling wind. The asymmetry causes the streamlines to be elliptical so that a net poleward current occurs across the vortex (see Chapter 4.3). This current supports poleward propagation of the cyclone and advects moisture from low latitudes toward

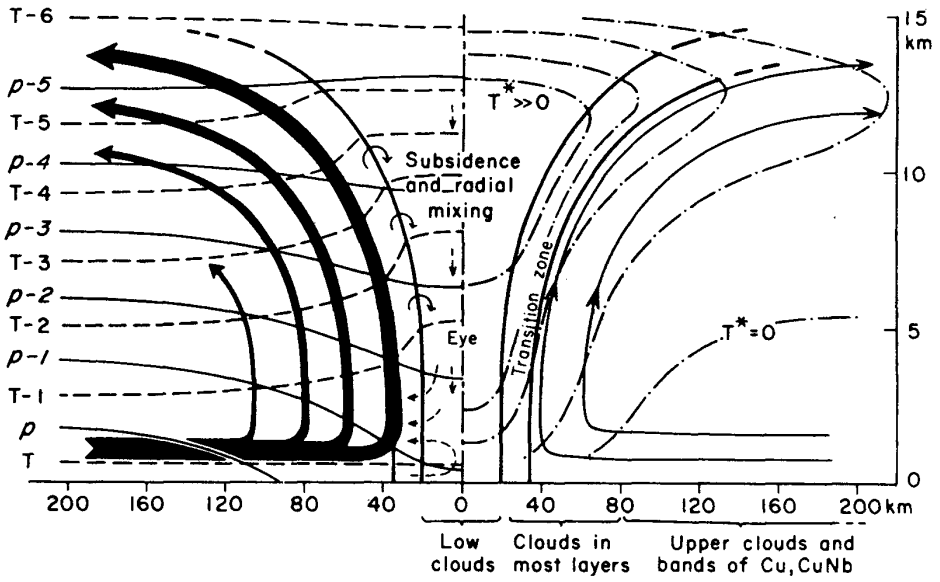

Fig. 2.1 Schematic cross section through the core of a tropical cyclone, showing the warm core, low pressure anomaly, and secondary circulation (Palmen and Newton 1969). Pressure (solid) and temperature (dashed) surfaces are shown on the left side, and temperature deviations from a standard atmosphere (dashed-dotted) are shown on the right side.

the center. In tropical cyclones that arise in the monsoon trough, the asymmetric flow is often associated with a band of convection that joins the cyclone to the trough (Holland 1984).

Topics treated in the rest of Chapter 2 are as follows: Chapter 2.2 deals with observational aspects of the evolution of the symmetric vortex. Chapter 2.3 treats the evolution of the asymmetric motions. Chapter 2.4 explores the tropical cyclone response to atmospheric, topographic, and oceanic forcing. A mathematical recapitulation of tropical cyclone dynamics appears in Chapter 2.5, and Chapter 2.6 is a summary.

2.2 AXISYMMETRIC VORTEX

Because the primary circulation is so strong in the cyclone core, it is possible to consider axisymmetric motions separately provided that account is taken of forcing by the asymmetric motions. The main balance of forces in the primary circulation is between the pressure gradient that tends to draw air into the vortex center and the Coriolis and centripetal accelerations required by a circular path around the center. The primary circulation evolves when heat and angular momentum sources (often due to asymmetric motions) force secondary circulations, which in turn redistribute heat and angular momentum. The secondary flow through a heat source is primarily vertical, and that through a momentum source is primarily horizontal (Fig. 2.3). Paradoxically, the induced secondary circulations in balanced flows tend to cancel the direct effect of forcing (Andrews and McIntyre 1976, 1978; Boyd 1976). For example, the work done by expansion in the updraft induced by a heat source nearly balances the actual heating. Similarly, a momentum source produces outflow that advects compensating low values of angular momentum from the vortex center. The streamlines of the secondary circulation form dipoles that extend outside the source, so that the source lies in intense flow between the oppositely rotating streamfunction gyres (Fig. 2.3). This flow emerges from the source, spreads outward through a large volume surrounding it, and converges back into it from the other side. Thus, compensating subsidence surrounds heating-induced updrafts, and compensating inflow lies above and below momentum-induced outflow.

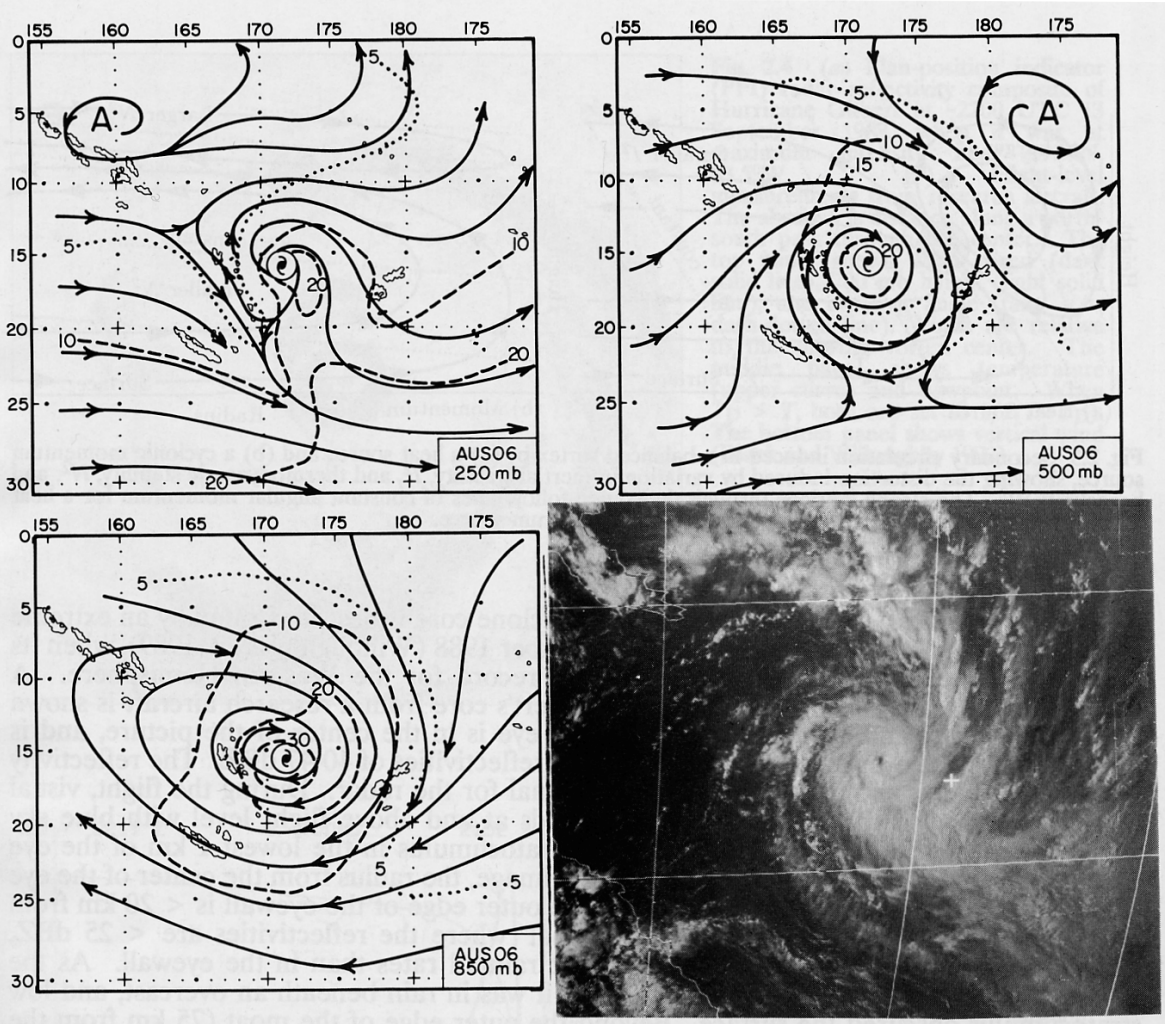

Fig. 2.2 Streamline isotach analyses at 250, 500, and 850 mb for a composite Southern Hemisphere tropical cyclone, together with a typical visible satellite image (after Holland 1984).

Gradients of angular momentum of the primary circulation can distort the dipoles. For a fixed static stability, the gyres tend to be elongated vertically when the radial gradient of angular momentum is large and elongated horizontally when the gradient of angular momentum is small. Vertical gradients of angular momentum due to vertical shears of the primary circulation deflect updrafts through the heat sources from the vertical because the path of least resistance for the warmed air lies along constant angular momentum surfaces. Similarly, horizontal temperature gradients due to vertical shears deflect the horizontal flow through momentum sources from the horizontal because the path of least resistance in this case lies along isentropes. Although the flow lies generally along the angular momentum or potential temperature surfaces, it does have a small component across them. It is advection by this component--not the direct forcing--that is the mechanism by which the primary circulation evolves. The swirling flow stays near gradient balance provided that the time scale that characterizes the forcing is longer than the orbital period of the primary circulation about the center.

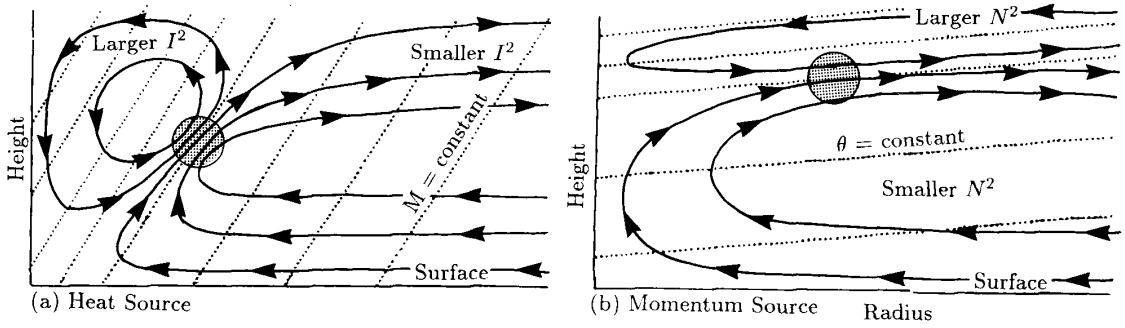

Fig. 2.3 Secondary circulation induced in a balanced vortex by (a) a heat source and (b) a cyclonic momentum source, showing the distortion induced by variation in inertial stability, I^2, and thermodynamic stability, N^2, and baroclinity, B^2. The strong motions through the source follow lines of constant angular momentum for a heat source and of constant potential temperature for a momentum source.

2.2.1 Intense tropical cyclones

The "classical" structure of the tropical cyclone core is best illustrated by an extreme case: Hurricane Gilbert at 2200 UTC 13 September 1988 (Willoughby *et al.* 1989), when its minimum sea-level pressure of 888 hPa set a record for the Western Hemisphere. A composite of radar reflectivity observed in Gilbert's core from a research aircraft is shown in Fig. 2.4 (Black and Willoughby 1992). The eye is in the center of the picture, and is surrounded by the eyewall with maximum radar reflectivities of 40-47 dBZ. The reflectivity in the eye is below the minimum detectable signal for the radar. During the flight, visual observation showed the eye to be free of clouds at and above flight level with blue sky visible overhead. Below flight level, broken stratocumulus in the lowest 1 km of the eye partially obscured the sea surface. In the radar image, the radius from the center of the eye to the inner edge of the eyewall is ~ 8 km. The outer edge of the eyewall is < 20 km from the center. Surrounding the eyewall is a "moat" where the reflectivities are < 25 dBZ, which is equivalent to a factor of > 100 lower rainfall rates than in the eyewall. As the aircraft flew across the moat at 3 km altitude, it was in rain beneath an overcast, and low stratocumulus obscured the surface. Beyond the outer edge of the moat (75 km from the center), the radar image shows precipitation organized into spirals that appear to be coalescing into a second ring of convection around the inner eye. Whereas the maximum reflectivities in the spirals are ~ 45 dBZ, which is a value comparable with that in the eyewall, reflectivities are $\leq$ 30 dBZ over much of the area outside the moat.

Radar shows patterns of precipitation, but radar images also contain important clues for visualization of the flow. Echo-free areas, such as the eye and the moat, generally indicate vortex-scale descent. The highly reflective echoes contain both convective updrafts and precipitation-induced downdrafts. The individual echoes may be arranged in rings that encircle the center or in open spirals. The lower reflectivities over most of the rings and spirals are stratiform rain falling from overhanging anvil cloud; the higher reflectivities are embedded convective cells. Based upon a typical radar reflectivity-rainfall relationship [$Z = 300R^{1.35}$, where Z is reflectivity (mm^6 m^{-3}) and R is rainrate (mm h^{-1}); Jorgensen and Willis 1982], R is < 4 mm h^{-1} in the stratiform areas and > 45 mm h^{-1} in the strong convection, which typically covers only a few percent of the TC as a whole.

Corresponding radial profiles of flight-level wind, 700 mb height, temperature, and dewpoint observed by the aircraft are shown in Fig. 2.4b. The strongest horizontal wind (> 80 m s^{-1}) is in the eyewall, only 12 km from the calm at the axis of rotation. Outside the eyewall, the wind drops abruptly to ~ 30 m s^{-1} at the outer edge of the moat and then

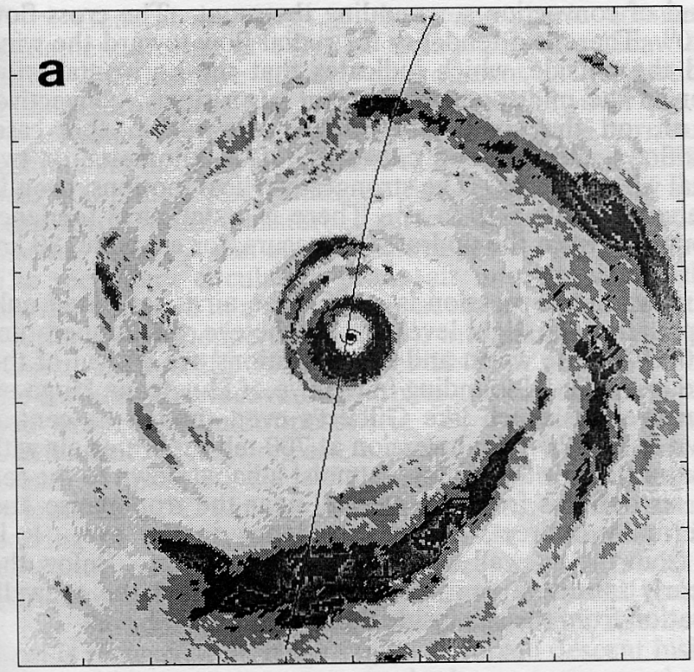

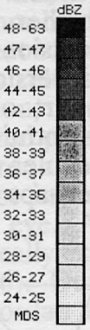

Fig. 2.4 (*a*) Plan-position indicator (PPI) radar reflectivity composite of Hurricane Gilbert at ~2200 UTC 13 September 1988, when it was at maximum intensity near 19.9°N, 83.5°W. (*b*) Flight-level measurements from research aircraft. The abscissa is distance along a north-south pass through the center. The top panel shows wind speed (dark solid line), 700 mb height (light solid line), and crossing angle ($\tan^{-1} u/v$, dash-dotted line). Winds are relative to the moving vortex center. The middle panel shows temperature (upper curve) and dewpoint. When $T_D > T$, both are set to $1/2(T+T_D)$. The bottom panel shows vertical wind (Black and Willoughby 1992).

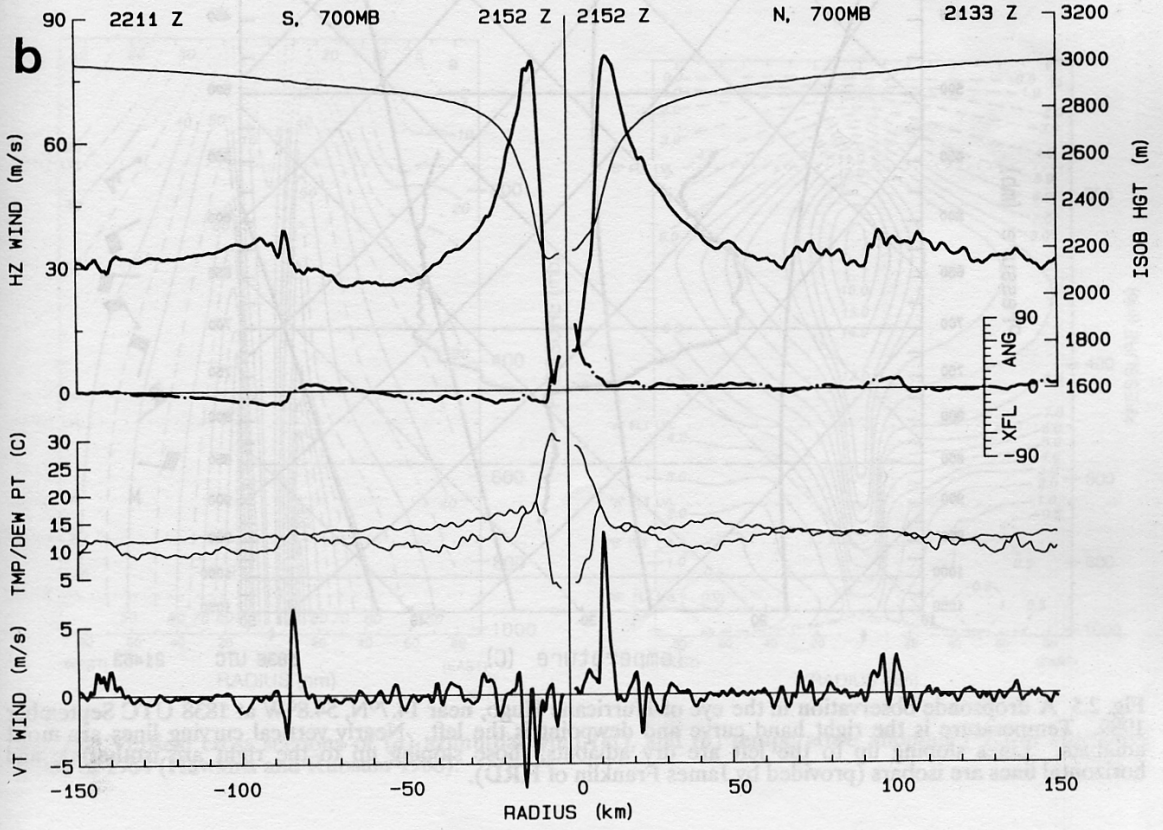

rises to 35 m s^{-1} in the partial band of convection surrounding the moat. The cross-flow angle ($\tan^{-1} u/v$) at 700 mb is < 10°. There is a tendency for radial flow toward the wind maxima from both the inside and the outside, which indicates that the horizontal wind converges into these features, even in the midtroposphere. Not surprisingly, convective-scale vertical motions--updrafts, or, on the south side of the eyewall in this case, downdrafts--often lie where the inflows and outflows converge just a kilometer or two radially outward from the horizontal wind maxima. The strongest vertical motions, even in this extraordinarily intense hurricane, are only 5-10 m s^{-1}. There is a statistical tendency for the downdrafts to lie radially outward from the updrafts, as occurs, for example, 80 km south of Gilbert's center.

Over most of Fig. 2.4b, the dewpoint depression is ~ 4°C. The air is saturated only where convective vertical motions pass through flight level. Inside the eye, the temperature is > 28°C and the dewpoint is < 0°C. These warm and dry conditions are typical of the eyes of extremely intense TCs (Jordan 1961). A sounding in the eye of Hurricane Hugo on 15 September 1989, when its structure was much like Gilbert's even though its central pressure was 34 mb higher, is shown in Fig. 2.5. An inversion at 700 mb separates air with ~ 20°C dewpoint depression from saturated air that follows a moist adiabat down to the sea surface. Above the inversion, the air detrains from the eyewall near the tropopause and flows downward as part of a thermally indirect, forced subsidence in the eye. It is moistened a little by entrainment from the eyewall and evaporation of virga. Below the inversion, the air is cooler and nearly saturated as a result of inflow under the eyewall, inward mixing, and perhaps evaporation from the sea inside the eye.

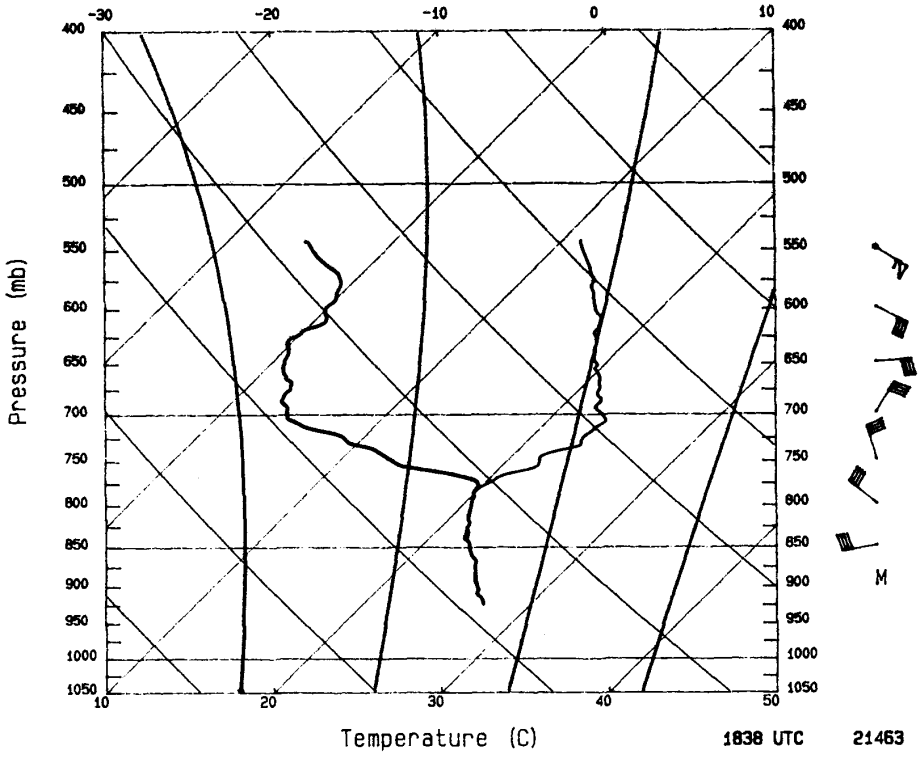

Fig. 2.5 A dropsonde observation in the eye of Hurricane Hugo, near 14.7°N, 54.8°W at 1838 UTC September 1989. Temperature is the right hand curve and dewpoint is the left. Nearly vertical curving lines are moist adiabats. Lines sloping up to the left are dry adiabats; those sloping up to the right are isotherms; and horizontal lines are isobars (provided by James Franklin of HRD).

General warming of the tropospheric column by latent heat release is the fundamental cause of TCs' low central pressure (Shaw 1922; Palmen 1948). The pressure deficit (δp) relative to the environment is proportional to the equivalent potential temperature excess ($\delta \theta_e$) averaged vertically over the depth of the troposphere $\delta p = -2.5 \delta \theta_e$ (Riehl 1963). In a composite analysis of the hurricane core (Gray and Shea 1973), θ_e just outside the eyewall is 358°K at the surface and 335°K at the midtropospheric minimum near 600 mb. These values are respectively > 10°K and > 5°K higher than those at the same levels in the undisturbed surroundings. In the boundary layer beneath the eyewalls of intense TCs, θ_e can easily reach values > 370°K as a result of heat transfer from the sea. The secondary circulation draws air into the vortex throughout the lower troposphere, carries it upward in a narrow ring at the eyewall, where the moisture condenses (Wood and Wexler 1945; Deppermann 1946), and exhausts it from the vortex near the tropopause (Durst and Sutcliffe 1938; Sawyer 1947) at potential temperatures nearly equal to θ_e at the surface. Convective overturning and dry turbulent mixing increase θ_e at middle levels and erode the midtropospheric θ_e minimum (Frank 1977b, 1984). The rate of condensational heat release, based upon a rainfall rate of 2 mm h^{-1} within 100 km of the center, is about 5 x 10^{13} W (Marks 1985), which is enough heat to warm the atmospheric column at 12°C per day. Although most of the latent heat release balances adiabatic cooling in the ascending branch of the secondary circulation, condensational heating concentrated in the cores of rapidly deepening TCs with observed pressure falls > 2 mb h^{-1} (Holliday and Thompson 1979) must support actual temperature increases > 10°C per day.

Paradoxically, much of the temperature rise occurs not in the eyewall where the heat is released, but in the region of forced descent inside the eye. As shown in Fig. 2.6b, the resulting temperature excess in the upper troposphere typically exceeds 10-15°C (Riehl 1948; Hawkins and Rubsam 1968; Hawkins and Imbembo 1976). Outside the eye, most of the temperature excess is confined to the upper troposphere (Jordan and Jordan 1954;

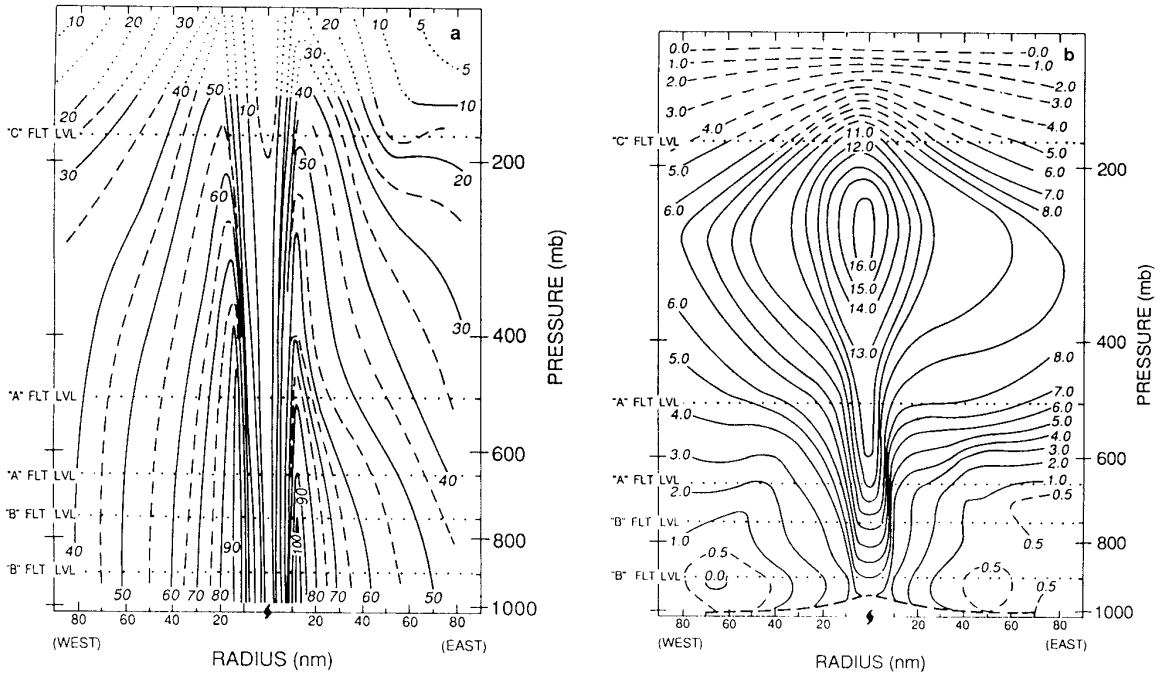

Fig. 2.6 Vertical cross sections of (*a*) azimuthal wind (kt), and (*b*) temperature anomaly (°K) in Hurricane Hilda of 1964 (Hawkins and Rubsam 1968).

Jordan 1958). The primary circulation (Fig. 2.6a) is strongest just above the frictional boundary layer. Below 500 mb, it has little vertical shear, but in the upper troposphere, it becomes weaker and less symmetric, and the radial outflow is a large fraction of the swirling motion. Near the tropopause beyond 200 km radius, the vortex turns anticyclonic (Jordan 1952, Koteswaram 1967) because of angular momentum loss to the sea on the inflow leg of the secondary circulation (Riehl 1963).

In Gilbert (Fig. 2.4b), the strongest radial gradient of 700 mb height roughly coincides with the maximum swirling wind, which suggests that the wind may be in gradient balance with the mass field. The gradual evolution and circularity of the lower-tropospheric vortex support the notion of gradient balance. Although the idea also has some observational basis (La Seur and Hawkins 1963; Hawkins and Rubsam 1968; Willoughby 1979, 1990b, 1991), some authors still dispute it (Gray 1991). Theoretical arguments aside, gradient balance prevailed in the midtroposphere in Gilbert to within a root-mean-squared deviation of $\pm$ 4 m s^{-1} (Fig. 2.7). Despite the possibility of deviations from balance where radial accelerations are large, such as where the frictional inflow decelerates under the eyewall, balanced models seem to explain many aspects of the evolution of axisymmetric TCs (Smith 1981; Shapiro and Willoughby 1982; Schubert and Hack 1982).

Figure 2.8 illustrates a schematic secondary circulation in a TC such as Gilbert (Willoughby *et al.* 1982; Jorgensen 1984a,b; Marks and Houze 1987). This circulation is forced by an intense frictional destruction of angular momentum at the surface, a strong, concentrated condensational latent heat release in the inner eyewall, weaker heating in the outer eyewall, extensive but weak cooling caused by frozen precipitation melting along the radar brightband, and similarly extensive and weak heating due to condensation and freezing in the anvil above the brightband. Since the diagnostic Eliassen equation for the secondary circulation (described in Chapter 2.5.2) is linear, the total secondary circulation

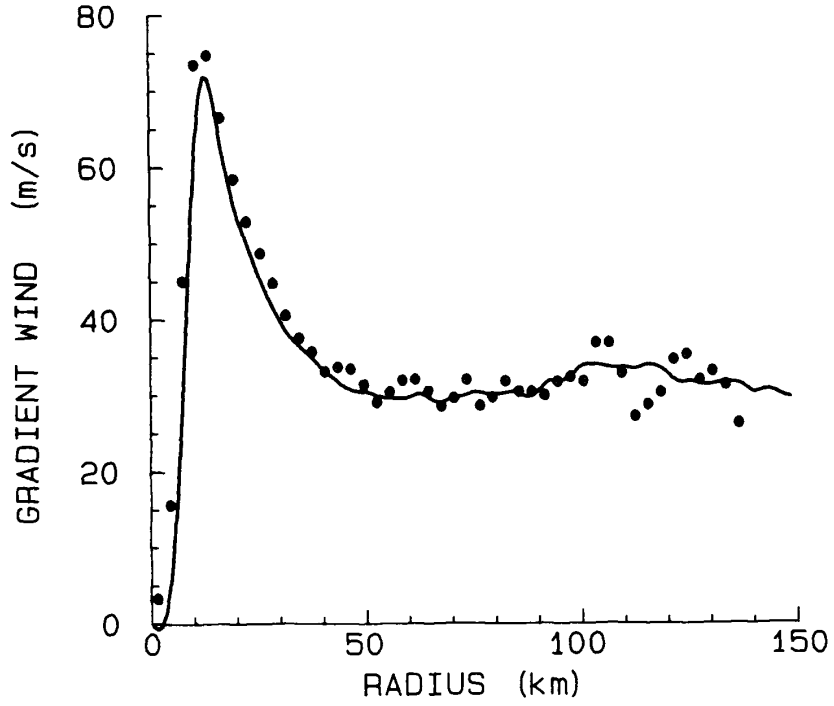

Fig. 2.7 Axisymmetric swirling wind (solid curve) and gradient wind computed every 5 km (circles) at 700 mb in Hurricane Gilbert on 13 September 1988 (Willoughby 1991).

is a superposition of the responses to these forcings. The streamfunction is the sum of the following parts: half a horizontal momentum-sink dipole in which the inflow jet is bisected by the sea surface; two vertical heat-source dipoles with updrafts that coincide with the inner and outer eyewalls; and two more thermodynamically forced dipoles due to the diffuse heating above and cooling below the 0°C isotherm in the stratiform area.

The inflow near the surface supplies only enough angular momentum to balance the frictional loss to the sea. This constraint is so strong that the inward mass flux is dominated by the surface stress and is not sensitive to the vertical structure of the turbulence (Leslie and Smith 1970). The latent heat that the inflowing air draws from the warm sea is the energy source for the updrafts in the eyewalls. Without condensational heating in the eyewalls, air converged in the surface layer would rise to the top of the friction layer and flow outward at the top of the frictional boundary layer instead of at the tropopause (Willoughby 1979). Both frictional surface convergence and heat transfer to the inflowing air are essential to maintenance of the deep secondary circulation.

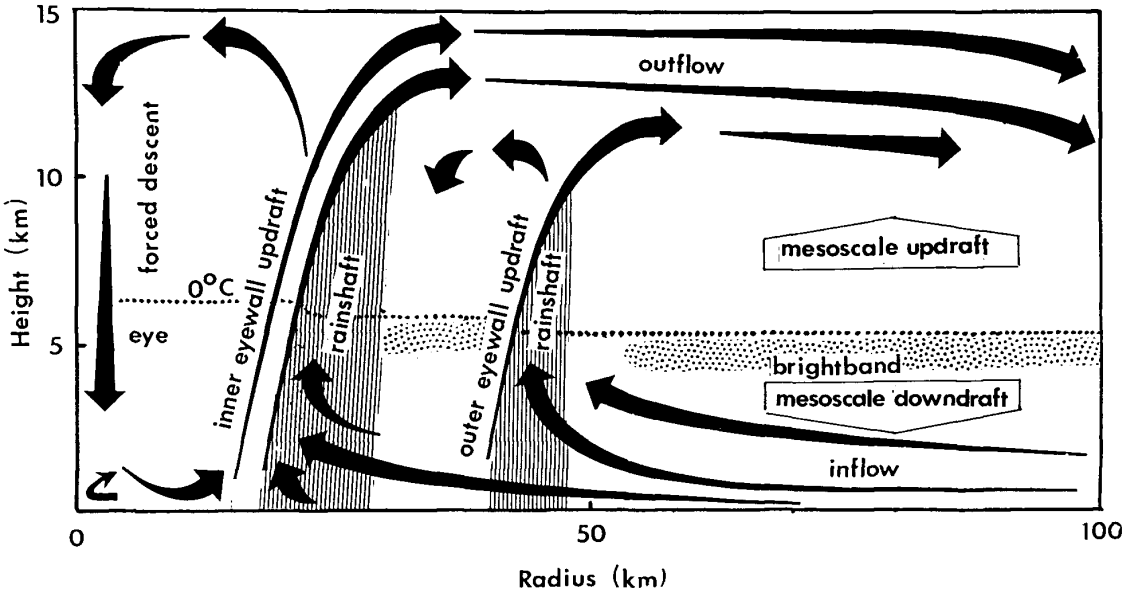

Fig. 2.8 Schematic of the secondary circulation and precipitation distribution for a tropical cyclone similar to Hurricane Gilbert at the time in Fig. 2.4 (Willoughby 1988).

The low-level inflow in the heating-induced thermally direct gyres in Fig. 2.8 is distinct from the frictional inflow (Frank 1977b, 1984). The swirling wind in the friction layer is generally a little weaker than that just above. Thus, only the heating-induced inflow can supply an excess of angular momentum beyond that required to balance frictional loss (Ooyama 1982). Observations show that the eyewall updrafts slope outward along constant angular momentum surfaces (Jorgensen 1984a,b; Marks and Houze 1987). The updraft slope from the vertical is the ratio of the vertical shear to the vertical component of the vorticity (Palmen 1956) and has typical values of 30°-60° (Black 1993), contrary to claims that eyewalls are vertical (Jordan *et al.* 1960; Shea and Gray 1973).

Outside the eye, latent heat release above the 0°C isotherm drives mesoscale updrafts. Below the 0°C isotherm, condensate loading and cooling due to melting of frozen hydrometeors drive mesoscale downdrafts. The mesoscale vertical velocities are typically tens of centimeters per second, and are large enough to appear in composite analyses of airborne Doppler radar observations (Marks and Houze 1987).

The secondary circulation controls the distribution of hydrometeors and radar reflectivity. Ascent is concentrated in convective updraft cores, which typically cover 10% of the area in the vortex core and more than half of the eyewall. The vertical velocity in the strongest 10% of the updraft cores averages 3-5 m s^{-1} (Jorgensen *et al.* 1985). Except for "supercells" sometimes observed in tropical storms (Gentry *et al.* 1970; Black 1983), the "hot towers" with updrafts > 20 m s^{-1} once thought to dominate vertical motions in hurricanes (Malkus 1959; Riehl and Malkus 1961; Malkus and Simpson 1964) appear to be rare. Much of the condensate falls out of the outwardly sloping updrafts, so that the rainshafts are outside and below the locus of ascent. The eyewall accounts for 25%-50% of the rainfall in the vortex core, but perhaps only 10% of the rainfall in the vortex as a whole (Marks 1985; Burpee and Black 1989). In the rainshafts, precipitation loading and, to a lesser extent, evaporation force convective downdrafts of a few meters per second (Jorgensen *et al.* 1985). Any condensate that remains in the updrafts is distributed horizontally in the upper troposphere by the outflow. It forms the central dense overcast that usually covers the TC core, and much of it ultimately falls as snow to the melting level where it forms the radar brightband (Jorgensen 1984a; Marks and Houze 1987). Nearly all the updrafts glaciate by -5°C because of ice multiplication and entrainment of frozen hydrometeors (Black and Hallett 1986).

Above the boundary layer, the secondary circulation and distributions of radar reflectivity and hydrometeors are much like those in a tropical squall line (Houze and Betts 1981). They have the same extensive anvil, mesoscale up- and downdrafts, and brightband. The boundary layer flows and energy sources are, however, much different. As a squall line propagates, it draws its energy from the water vapor stored in the undisturbed boundary layer ahead of it, and leaves behind a cool wake that is capped by warm, dry mesoscale downdraft air under the anvil. As shown below, an eyewall propagates inward, but draws energy primarily from behind (outward) rather than ahead (inward). Frictional inflow feeds the updraft with latent heat extracted from the sea under the anvil. The reason for the difference between an eyewall and a squall line is the increased rate of air--sea interaction (Rotunno and Emanuel 1987) in the strong primary circulation of a TC.

2.2.2 Convective rings

In each of the concentric eyewalls shown in Figs. 2.4 and 2.8, convective heating causes a streamfunction dipole with a thermally direct gyre outside the eyewall and a thermally indirect gyre inside the eyewall. The direct gyres have inflow near the surface, ascent at the eyewall, and outflow near the tropopause. The indirect gyres have low-level outflow that joins the eyewall updraft from the eye, inflow that diverges from the eyewall updraft into the eye near the tropopause, and forced descent at the center of the eye. Ascent of warm air in the direct gyres produces kinetic energy and descent of warm air in the indirect gyres consumes it. In the part of the vortex occupied by the direct gyres, the swirling wind decreases outward from the center, so that the inertial stability is smaller than in the area occupied by the indirect gyre, where the swirling wind increases with distance from the center (see Fig. 2.3a). Since the thermodynamic stability is nearly constant, variation of the inertial stability controls the shape of the streamfunction gyres. Outside the eye, the secondary circulation is strong, predominantly horizontal, and extends to large radius. Inside the eye, the secondary circulation is weaker, more nearly vertical, but concentrated horizontally. This discussion makes it clear that the descent in the eye is primarily a response to condensational heating at the eyewall (Willoughby 1979), and not a result of inward momentum diffusion or "overshooting" of the inflowing air, which might lead to "supergradient" winds that "centrifuge" air out of the eye (Malkus 1958; Kuo 1959; Gray and Shea 1973). As Figs. 2.4 and 2.8 are drawn, the inner eyewall is the stronger. When concentric eyewalls exist, the outer eyewall's indirect cell usually causes the inner eyewall to weaken by forcing descent and low-level outflow around the vortex center (Willoughby *et al.* 1982; Shapiro and Willoughby 1982).

The term "convective ring" (Willoughby *et al.* 1982) describes coherent, inward propagating rings of convection associated with local maxima of the swirling wind. It includes inner eyewalls and outer concentric eyewalls. The observed inward motion of convective rings stems from the asymmetry between the thermally direct and indirect gyres. A condensational heat source near the tangential-wind maximum induces large total subsidence outward from the wind maximum and smaller total subsidence inward from the maximum. On the outside, the subsidence is distributed over a wide area; on the inside, it is concentrated near the heat source. The subsidence-induced adiabatic warming is stronger radially inward from the ring, so that a sharp contrast of hydrostatic isobaric height falls forms across the wind maximum. Through the gradient wind relation, the tangential wind increases most rapidly at and just inward from the maximum. Kinematically, the inward propagation speed of the wind maximum may be expressed as the ratio of the time rate of increase of the swirling wind to its radial gradient evaluated on the inward side of the wind maximum.

The intensification of Hurricane Danny (Willoughby 1990a) illustrates development of a single convective ring. Danny became a hurricane on 14 August 1985 in the Gulf of Mexico and made landfall on the Louisiana coast the next day (Case 1986). Research aircraft monitored Danny for > 27 h as the cyclone tracked northwestward toward landfall. Danny's convective ring (Fig. 2.9a) was not a locus of uniform mesoscale ascent, but rather a collection of convective cells arranged in bands, much like the outer eyewall of Gilbert in Fig. 2.4a. At 1505 UTC 14 August, Danny's strongest winds lay more than 120 km from the center (Fig. 2.9b) and the convection was poorly organized. Over ~ 20 h, the wind on the inward side of the maximum increased, which caused the radius of maximum wind to contract to 60 km and the maximum wind to increase from 18 to 45 m s^{-1} (Fig. 2.9b) by the time of landfall. The contraction of the eyewall, the increase of the maximum wind, and the sharpening of the wind profile all agree with predictions of the balanced Eliassen model to be described in Chapter 2.5.2.

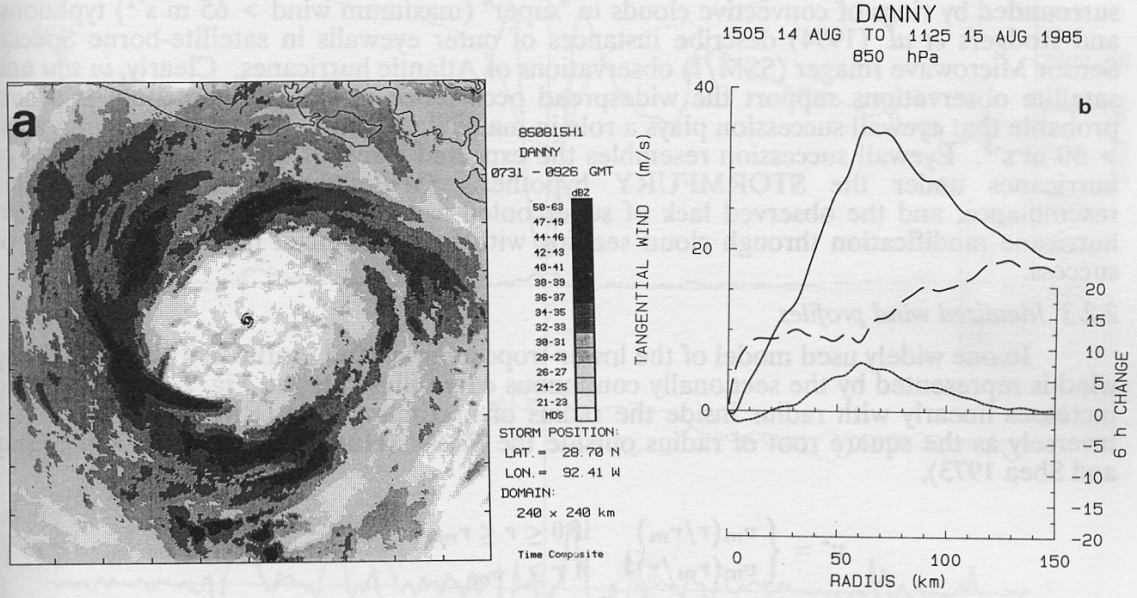

Fig. 2.9 (*a*) Radar reflectivity composite as in Fig. 2.4a, except in Hurricane Danny near 28.7°N, 92.41°W at ~0900 UTC 15 August 1985. (*b*) Evolution of 850 mb tangential wind in Danny between 1500 UTC 14 August (dashed) and 1125 UTC 15 August (solid), as well as the difference between the curves normalized to a 6 h interval (dotted) (Willoughby 1990a).

Gilbert's outer eyewall followed a development similar to Danny's eyewall. Over a period of 12 h since the time of Fig. 2.4a, the convection became organized into a distinct ring with a sharp inner edge (Fig. 2.10a). The outer wind maximum increased from 35 m s^{-1} to nearly 50 m s^{-1} while the inner wind maximum declined to 70 m s^{-1} (Fig. 2.10b). In addition, the dewpoint depression in the eye dropped to 10°C as a result of the weakening of the subsidence in the original eye as it began to feel the influence of the outer eyewall. In both Danny and Gilbert, a loose circular arrangement of convection became organized into a convective ring. Gilbert's outer eyewall was in the process of replacing the original eyewall when the TC made landfall on the Yucatan peninsula.

As the inner ring weakens in these situations, the minimum sea-level pressure will increase if the pressure rise due to the inner ring's destruction is greater than the pressure fall due to the outer ring's continuing intensification (Willoughby *et al.* 1982). In Gilbert's case, the eyewall replacement coincided with passage over the Yucatan and reemergence over the Bay of Campeche where the oceanic thermocline was shallower so that the hurricane winds cooled the sea surface through mixing and upwelling (Shay *et al.* 1992). The next day, the wind profile (Fig. 2.11b) was much flatter with maximum wind < 40 m s^{-1} at the old outer eyewall (Black and Willoughby 1992). The original inner eyewall was still visible on radar (Fig. 2.11a), but it enclosed no detectable anomalies of temperature or humidity, and no strong convective updrafts remained. Flat wind profiles as in Fig. 2.11b characterize TCs that have lost vigorous convection after an eyewall replacement or motion over cold water, as well as some developing depressions or tropical storms that have not yet formed convective rings, e.g., Danny before the events portrayed in Fig. 2.9.

Other examples of eyewall successions include Hurricane Beulah of 1967 (Hoose and Colon 1970), Typhoon Gloria of 1974 (Holliday 1977) and Hurricanes Allen of 1980 (Willoughby *et al.* 1982), Alicia of 1983, Diana of 1984, Gloria of 1985 (Willoughby 1990a), and Andrew of 1992. The filling of minimum sea-level pressure may be as large as 30 mb, and the time required for a cycle of weakening and reintensification ranges from a few hours to more than a day. Dvorak (1975) describes circular central dense overcasts surrounded by rings of convective clouds in "super" (maximum wind > 65 m s^{-1}) typhoons, and Rodgers *et al.* (1994) describe instances of outer eyewalls in satellite-borne Special Sensor Microwave Imager (SSM/I) observations of Atlantic hurricanes. Clearly, *in situ* and satellite observations support the widespread occurrence of this phenomenon. It seems probable that eyewall succession plays a role in many, if not most, TCs with maximum wind > 50 m s^{-1}. Eyewall succession resembles the expected result of artificial modification of hurricanes under the STORMFURY hypothesis (Willoughby *et al.* 1985). This resemblance, and the observed lack of supercooled water in TCs, makes it unlikely that hurricane modification through cloud seeding with freezing nuclei has much prospect of success.

2.2.3 Idealized wind profiles

In one widely used model of the lower-tropospheric wind profile in TCs, the swirling wind is represented by the sectionally continuous curve illustrated in Fig. 2.12a. The wind increases linearly with radius inside the radius of maximum wind (RMW) and decreases inversely as the square root of radius outside the RMW (Hughes 1952; Riehl 1963; Gray and Shea 1973),

$$v^* = \begin{cases} v_m(r/r_m) & \text{if } 0 \le r \le r_m, \\ v_m(r_m/r)^{\frac{1}{2}} & \text{if } r \ge r_m \end{cases} \tag{2.1}$$

where v^* is the swirling wind, r is radius, r_m is the RMW, and v_m is the maximum wind. Because the swirling wind decreases more slowly than r^{-1}, the angular momentum decreases with radius and the wind profile is inertially stable. If the wind is assumed to be in cyclostrophic balance, $v_c^2/r = \rho_0^{-1}\partial p/\partial r$, radial integration of (2.1) from a large radius

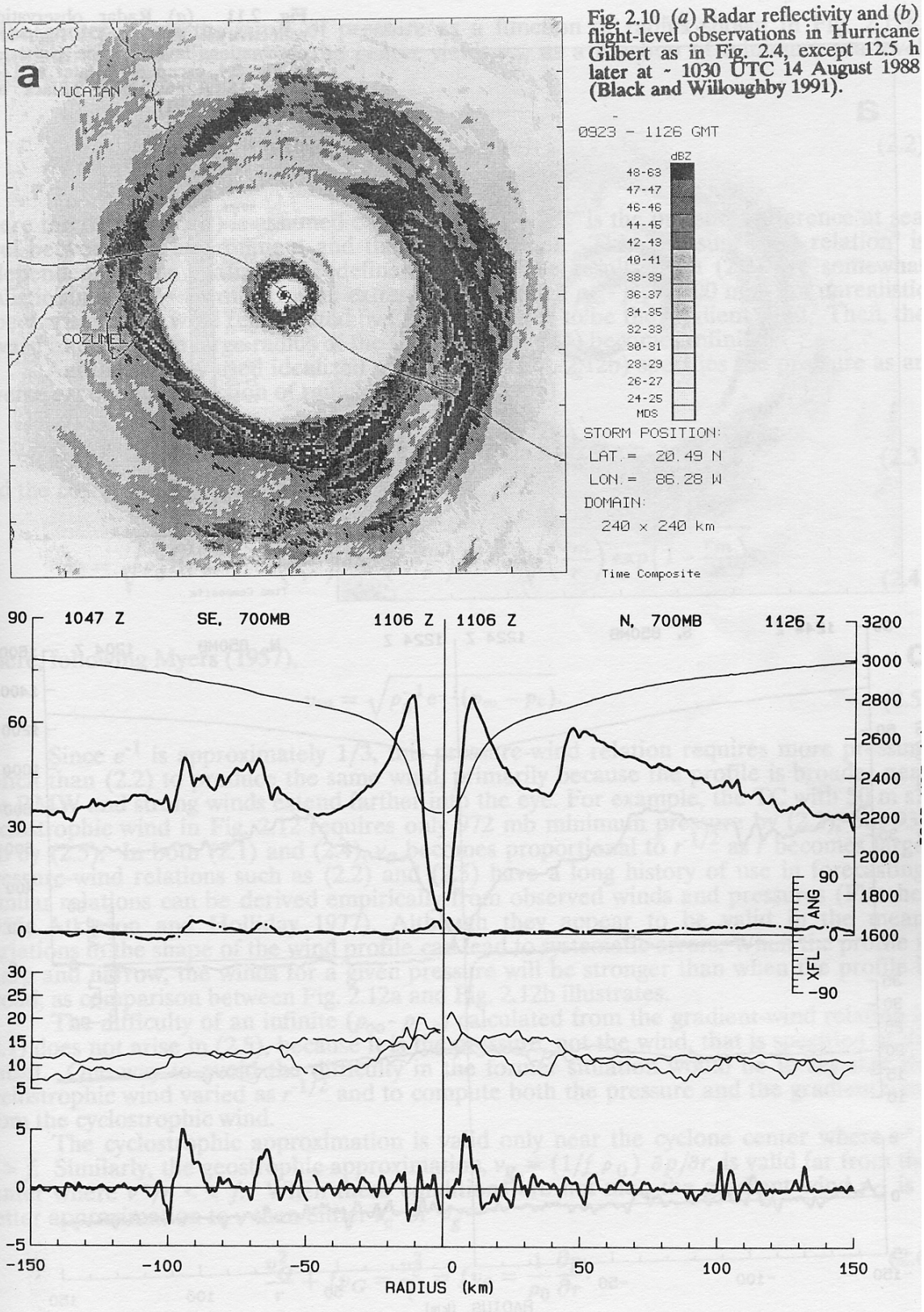

Fig. 2.10 (*a*) Radar reflectivity and (*b*) flight-level observations in Hurricane Gilbert as in Fig. 2.4, except 12.5 h later at ~ 1030 UTC 14 August 1988 (Black and Willoughby 1991).

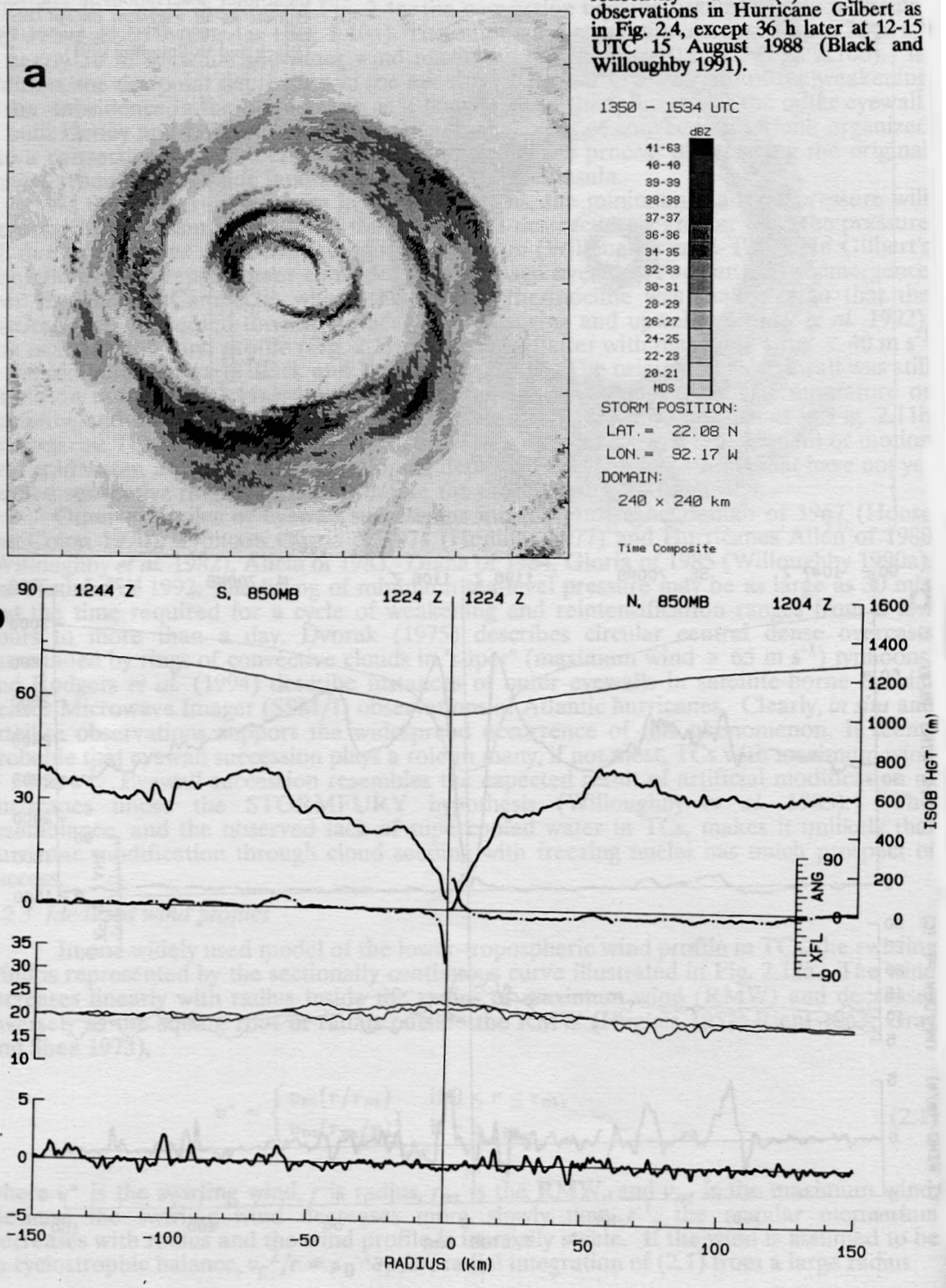

Fig. 2.11 (*a*) Radar observations reflectivity and (*b*) flight-level observations in Hurricane Gilbert as in Fig. 2.4, except 36 h later at 12-15 UTC 15 August 1988 (Black and Willoughby 1991).

to the center yields the curve of pressure as a function of radius shown in Fig. 2.12a. Continuation of the integral to the center yields v_m as a function of minimum sea-level pressure (MSLP)

$$v_m = \sqrt{\frac{2}{3}\rho_0^{-1}(p_\infty - p_c)}, \tag{2.2}$$

where the density (ρ_0) is assumed constant and $p_\infty - p_c$ is the pressure difference at sea level between the environment and the cyclone center. This "pressure-wind relation" is independent of the spatial scale defined by r_m. The results from (2.2) are somewhat realistic since v_m = 82 m s^{-1} for an extreme TC in which $p_\infty - p_c$ = 100 mb. An unrealistic aspect arises if the wind represented by (2.1) is assumed to be the gradient wind. Then, the inward integral from large radius of the Coriolis term (fv^*) becomes infinite.

Another widely used idealized wind profile (Fig. 2.12b) specifies the pressure as an inverse exponential function of radius (Schloemer 1956)

$$p = p_c + (p_\infty - p_c)\exp\left(-\frac{r_m}{r}\right), \tag{2.3}$$

and the corresponding wind is

$$v_c = \sqrt{\rho_0^{-1}(p_\infty - p_c)\left(\frac{r_m}{r}\right)\exp\left(-\frac{r_m}{r}\right)} = v_m\sqrt{\left(\frac{r_m}{r}\right)\exp\left(1 - \frac{r_m}{r}\right)}, \tag{2.4}$$

where, following Myers (1957),

$$v_m = \sqrt{\rho_0^{-1}e^{-1}(p_\infty - p_c)}. \tag{2.5}$$

Since e^{-1} is approximately 1/3, this pressure-wind relation requires more pressure deficit than (2.2) to produce the same wind, primarily because the profile is broader near the RMW and strong winds extend farther into the eye. For example, the TC with 50 m s^{-1} cyclostrophic wind in Fig. 2.12 requires only 972 mb minimum pressure by (2.2), but 938 mb by (2.5). In both (2.1) and (2.4), v_c becomes proportional to $r^{-1/2}$ as r becomes large. Pressure-wind relations such as (2.2) and (2.5) have a long history of use in forecasting. Similar relations can be derived empirically from observed winds and pressures (Fletcher 1955; Atkinson and Holliday 1977). Although they appear to be valid in the mean, variations in the shape of the wind profile can lead to systematic errors. When the profile is sharp and narrow, the winds for a given pressure will be stronger than when the profile is broad, as comparison between Fig. 2.12a and Fig. 2.12b illustrates.

The difficulty of an infinite ($p_\infty - p_c$) calculated from the gradient-wind relation in (2.1) does not arise in (2.5), because it is the pressure, not the wind, that is specified at the outset. One way to avoid the difficulty in the former situation would be to say that the cyclostrophic wind varied as $r^{-1/2}$ and to compute both the pressure and the gradient wind from the cyclostrophic wind.

The cyclostrophic approximation is valid only near the cyclone center where $v^*/r >> f$. Similarly, the geostrophic approximation, $v_g = (1/f\rho_0)\,\partial p/\partial r$, is valid far from the center where $v^*/r << f$. When these conditions are not met, the gradient wind v_G is a better approximation to v than either v_c or v_g

$$\frac{v_G^2}{r} + fv_G = \frac{v_c^2}{r} = fv_g = \frac{1}{\rho_0}\frac{\partial p}{\partial r}. \tag{2.6}$$

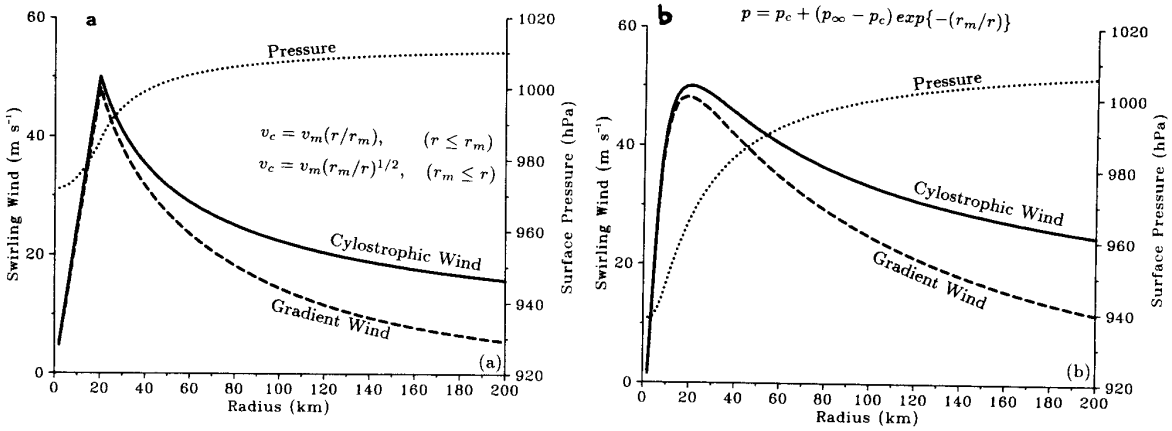

Fig. 2.12 Idealized profiles of cyclostrophic wind, sea-level pressure, and gradient wind computed from (*a*) equation (2.1) and (*b*) equation (2.3).

An informative solution of (2.6) for v_G is obtained after division through by v_G^2/r and v_C^2 and solving for $1/v_G$ with the quadratic formula, and inversion of the result

$$v_G = \frac{v_c}{\frac{1}{2R_c} + \sqrt{1 + \frac{1}{4R_c^2}}} \tag{2.7}$$

where $R_c = v_c/f_r$ is the Rossby number based upon the cyclostrophic wind such that $v_g = R_c v_c$. Where R_c is large near the cyclone center, v_G approaches v_c; where R_c is small far from the center, v_G approaches v_g. In Fig. 2.12b, the gradient winds are about 2 m s^{-1} weaker than the cyclostrophic winds at the RMW and about two-thirds of v_c where $R_c \sim 1$.

Holland (1980) elaborated on (2.3) by replacing (r_m/r) with $(r_m/r)^B$, where B was an empirically adjustable exponent. This modification allowed adjustment of the sharpness of the wind profile to fit the range of shapes found in nature, and profiles derived from it have been used with some success in forecasting (see Chapter 6.8.2). Nevertheless, idealized radial profiles have problems. They do not portray multiple wind maxima. Their integral properties, such as the total kinetic energy and angular momentum, tend to be infinite over infinite domains (although substitution of gradient winds for cyclostrophic winds as in (2.7) can keep integral values of kinetic energy bounded). The most serious problem, apart from the sharpening or broadening of the wind maximum achieved by changes in Holland's exponent, is that r_m determines the spatial scale of the entire vortex. Observations described in the next subsection demonstrate that the winds in the outer circulation often vary independently of the vortex core.

2.2.4 Outside the core

The outer wind profiles of TCs can be as diverse as those in the core (Fig. 2.13a). For this reason, it is important to distinguish between the "intensity" of the cyclone core and the "strength" of the outer circulation (Merrill 1984). As illustrated in Fig. 2.13b, intensity is conventionally measured in terms of maximum wind or minimum sea-level pressure; strength is a spatially-averaged wind speed over an annulus between 100 and 250 km from the cyclone center (Weatherford and Gray 1988a). Another useful parameter is size, which is variously defined as the average radius of the outer closed isobar (ROCI) or of gale force (17 m s^{-1}) wind. Size and strength are strongly correlated, but neither is strongly correlated with intensity.

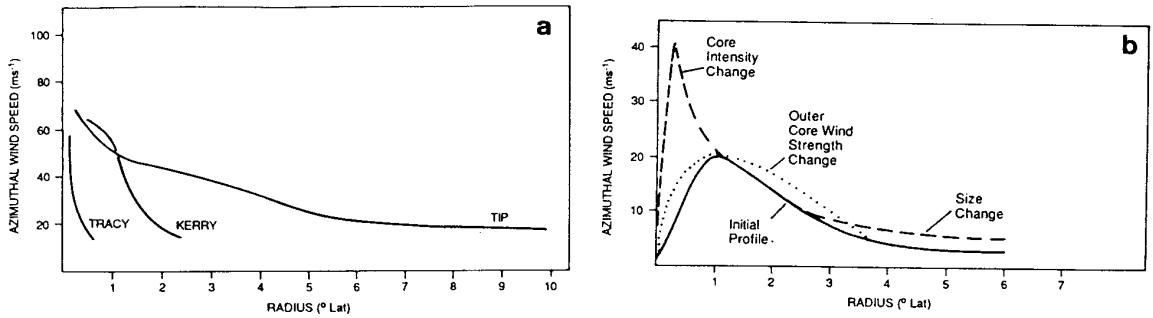

Fig. 2.13 (*a*) Radial profiles of low-level azimuthal winds in Cyclones Tracy and Kerry and Typhoon Tip (Holland and Merrill 1984). (*b*) A schematic of changes in core intensity, outer core strength and size of the azimuthal wind's radial profile (Merrill 1984).

The climatology of size is well established for the Atlantic and North Pacific (Merrill 1984; Brand 1972). On average, typhoons are 1.5° lat. larger than Atlantic hurricanes. Small (ROCI < 2° lat.) TCs are most frequent early in the season (August), and large (ROCI > 10° lat.) ones late in the season (October). Large TCs are most common at 30° N, which is the average latitude of recurvature. Small TCs have much smaller total angular momentum and lose less of it to friction than large ones. The angular momentum required for growth (increase in size) at climatologically typical rates is about the same as that required to balance friction, but significantly less than required to balance the Coriolis torque that converts relative angular momentum to planetary angular momentum over the volume of a TC moving poleward at a climatological speed. Generally, intensity changes require much smaller angular momentum imports than changes of size or strength.

The life cycle of an Atlantic TC (Merrill 1984) begins with a formative stage (see Chapter 3) during which the outer circulation contracts a little as the core intensifies. During the immature stage, the intensity increases to a maximum as the size remains constant. In the mature stage, the TC grows, but no longer intensifies. In the decaying stage, the inner core winds decrease as the circulation continues to grow. The ROCI typically is 2.5° lat. in the immature stage and twice that value in the decaying stage a week later. The maximum intensity, start of rapid growth, and recurvature of the track tend to coincide.

Detailed study of reconnaissance aircraft data from the western North Pacific confirms the low correlation between strength and intensity, and essentially no correlation between strength and intensity time changes (Weatherford and Gray 1988a,b). That is, strength is equally likely to increase or decrease as a typhoon intensifies. Commonly, intensification precedes strengthening, and weakening of the core precedes that of the outer circulation. Classification of the observations by eye size [small (radius $\leq$ 15 km), medium (16-30 km), large (30-120 km), and eyewall absent] reveals correlations between intensity and strength, even though none could be found for the sample as a whole. These correlations may become evident because eye size acts as a proxy for phase of the typhoon life cycles.

Convective rings may explain many aspects of this description. The "no eye" typhoons have a clear outer wind maximum at > 1° lat. radius. The case of Typhoon Owen's growth as its intensity decreased (Fig. 24 of Weatherford and Gray 1988a) is a clear example of an eyewall replacement. The life cycle might be interpreted in terms of the following convective ring paradigm. A TC intensifies with little change of size or strength as its original eyewall develops. It then strengthens as an outer eyewall forms. Strengthening and growth continue, but the intensity decreases as the inner eyewall

dissipates in an eyewall replacement. Intensification might resume again as the new eyewall becomes dominant, or the TC might weaken if the new eyewall fails to intensify as a result of environmental shear or lower sea-surface temperatures. Although none of these changes occurs at the same time, the cycle leaves the TC larger, stronger, and possibly more intense.

2.3 ASYMMETRICAL STRUCTURE

Spiral-shaped patterns of precipitation characterize radar and satellite images of tropical cyclones (Fig. 2.14). As indicated in Chapter 1.4, the earliest radar observations of TCs (Maynard 1945) detected these bands, which are typically 5-50 km wide and 100-300 km long (Wexler 1947). Nevertheless, many aspects of their formation, dynamics, and interaction with the symmetric vortex are still unresolved. The precipitation-free lanes between bands tend to be somewhat wider than the bands. The trailing-spiral shape of bands and lanes arises because the angular velocity of the vortex increases inward and distorts them into equiangular spirals (Abdullah 1966)

$$r = Ae^{-\alpha(\lambda-\lambda_0)}, \tag{2.8}$$

where α is the tangent of the "crossing angle" (the angle that the band makes with a circle around the origin, usually 10°-20°), r and λ are the radius and azimuth (reckoned cyclonically from north) of points on a band that also passes through a given point at $r=A$ and $\lambda = \lambda_0$(Hiser and Freseman 1959). Radar observers use transparent plastic overlays

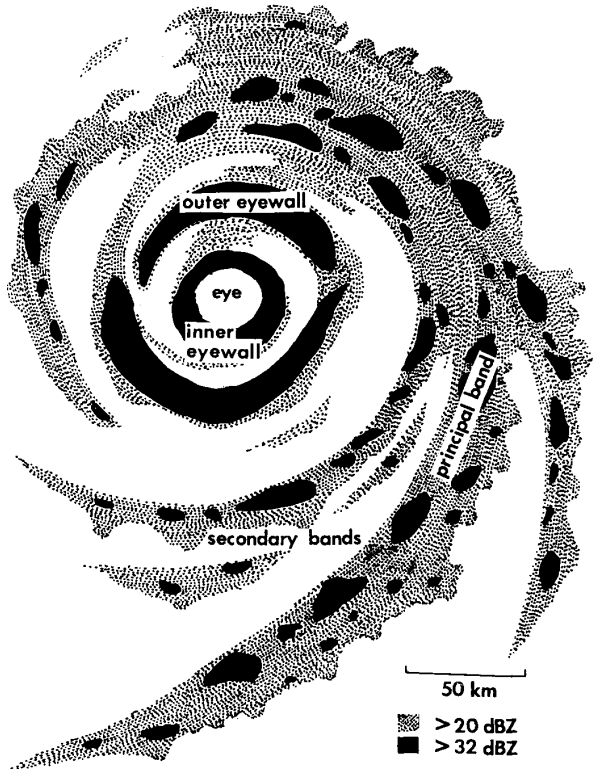

Fig. 2.14 Typical banded radar reflectivity pattern in a Northern Hemisphere tropical cyclone with 50-60 m s^{-1} maximum wind in a sheared environmental flow (Willoughby 1988).

with spirals calculated from (2.8) to locate the centers of TCs when some bands are visible at long range but the center is not. As the TC becomes more intense, the inward ends of the bands approach the center less steeply and then approximate arcs of circles (Malkus *et al.* 1961; Dvorak 1975). In these cases, (2.8) might be modified to

$$r = a + (A - a)e^{-\alpha(\lambda - \lambda_0)}, \tag{2.9}$$

where a is the radius at which the band approaches a circle. A dynamical distinction exists between convective bands that spiral outward from the center and convective rings that encircle the center. Because the bands often join a ring or appear to wrap around the center (Dvorak 1984), this distinction is often difficult to make in radar or satellite images.

Although precipitation in some bands is largely stratiform (Atlas *et al.* 1963; Marks 1985), condensation in most bands tends to be concentrated in convective cells rather than spread over wide mesoscale areas. Convective elements form near the inner, upwind edges of the bands, move through the bands, and dissipate on the outward, downwind edges (Ligda 1955a). As the cells cross the band, they also move inward along the band. The dissipating elements feed an extensive anvil and generate widespread stratiform precipitation through horizontal advection of convective debris. These observations make it appear that spiral bands are more like squall lines than linear gravity waves.

Dual-Doppler radar observations of a rainband in Supertyphoon Abby of 1983 confirmed inflow from the inward (concave) side, a locus of mesoscale ascent along the concave edge of the band, and a locus of mesoscale descent along the outer (convex) side (Ishihara *et al.* 1986). This pattern of inflow stemmed from the band's steep inward crossing angle of 25°. The roots of the updrafts lay in convergence between the swirling flow and gust fronts that are produced by the downdrafts. The updrafts leaned outward from the typhoon center toward the convex side of the band and fed an extensive anvil that spread downwind from the band. The band moved more slowly than the surrounding winds, i.e., it propagated upwind. Even though the band was over land at 36°N, the equivalent potential temperature at the surface was 355°, and this band should be considered representative of squall-line bands in hurricanes.

These Abby observations contrast with aircraft and radar observations of a "band" in Hurricane Floyd of 1981 (Barnes *et al.* 1983). In the Floyd case, the low-level air spiraled inward more steeply than the band, so that the band intercepted the radial inflow on its outer, convex side. The inflow passed under the anvil between the convective-scale, precipitation-driven downdrafts to feed an updraft on the inner, concave side of the band. As in Typhoon Abby, the updraft sloped outward over the downdraft and fed an anvil extending away from the TC center. The 20°K decrease in low-level θ_e across the band indicates that the band was a barrier to inflow. Independent observations in Hurricane Earl by Powell (1990a,b) confirmed the synthesis of Barnes *et al.*, and emphasized that cooling and shallowing of the boundary layer occurred as the vortex-scale inflow passed under or between the cells of the bands (Fig. 2.15). This reduction in boundary-layer energy may have inhibited convection nearer the center. Powell also noted that sometimes the band may draw air from both sides. An important difference between a convective ring and a spiral band is that the swirling wind feeds the updraft in a band from the concave side, whereas the radial flow feeds the updraft in a convective ring primarily from the convex side. By this distinction, the features that Barnes *et al.* and Powell describe are partial convective rings rather than spiral bands.

Some bands appear to move outward (Senn and Hiser 1959), while others maintain a fixed location relative to the translating TC center (Malkus *et al.* 1961; Ligda 1955b). Moving bands, and other convective features, are frequently associated with cycloidal motion of the TC center (Neuman and Boyd 1962; Jordan 1966; Muramatsu 1986), and intense asymmetric outbursts of convection (supercells) are observed to displace the TC center by tens of kilometers (Willoughby 1990a). A shallow-water barotropic vortex motion model forced by a mass source-sink dipole can simulate either cycloidal motions

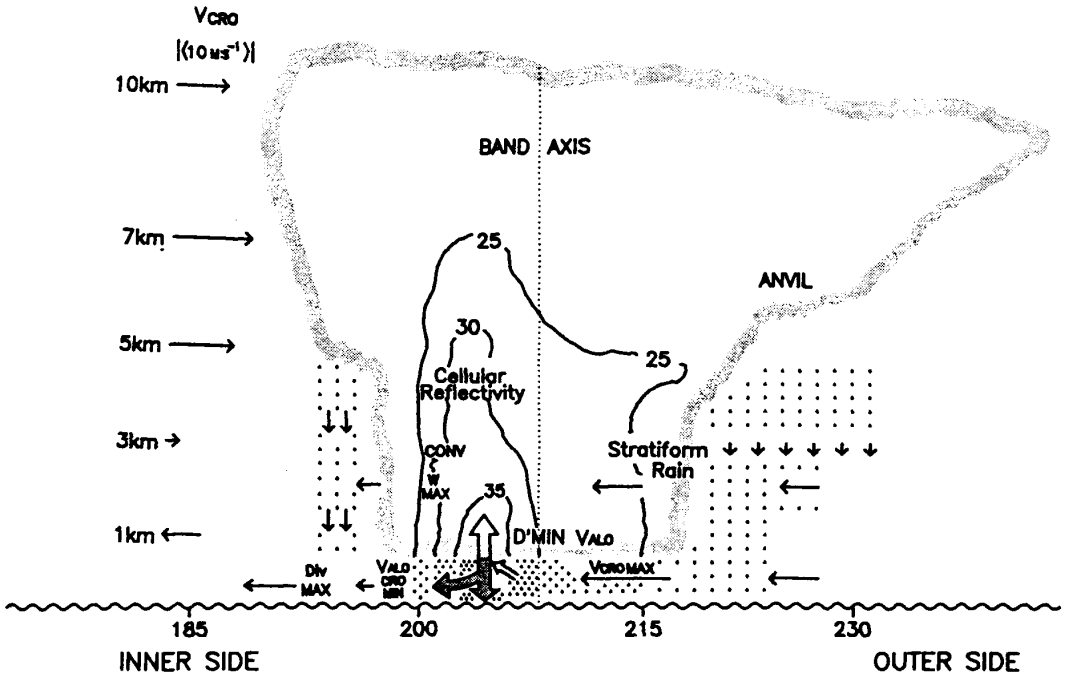

Fig. 2.15 Thermodynamic structure of a rainband in Hurricane Earl (1986). The gray outline shows the cloud boundary, and the contours show radar reflectivity. Heavy horizontal and vertical arrows indicate the cross-band (V_{CRO}) and convective vertical flows; lighter arrows indicate mesoscale subsidence (Powell 1990b).

when the dipole rotates or linear track displacements when it is fixed. The rotating dipole also generates outward-propagating, gravity-wave spirals (Willoughby 1992).

The bands observed by radar are often considered to be manifestations of internal gravity waves (Yamamoto 1963), but a difficulty with the gravity-wave model of spiral bands is the "frequency problem." It will be shown in Chapter 2.5.3 that internal gravity waves exist only in a band of Doppler-shifted frequencies between the local inertia frequency and the Brunt-Vaisala frequency. Only two classes of trailing-spiral, gravity-wave solutions lie within this band: waves with any tangential wavenumber that move faster than the swirling wind and waves with tangential wavenumber ≥ 2 that move more slowly than the swirling wind. Rapidly moving bands with outward phase propagation have been observed by radar. They propagate both wave energy and angular momentum outward, but do not draw much energy from the mean flow. Because they have large vertical group velocities, they should leak energy into the stratosphere rapidly. The outward-moving bands are thus more likely to be squall lines than linear gravity waves. The slowly-moving waves propagate wave energy and anticyclonic angular momentum inward, grow at the expense of the mean-flow kinetic energy (Kurihara 1976), and can reach appreciable amplitude if they are excited at the periphery of the TC. An alternate description for inward-propagating bands involves filamentation of potential vorticity (PV) from the TC environment or asymmetries in the radially shearing flow of the vortex (Guinn and Schubert 1993b). Asymmetric wave breaking and symmeterization of the PV surrounds the vortex core with a "surf zone" that bears a strong resemblance to Gilbert's outer convection as it was being organized into a concentric eyewall (Fig. 2.4a).

As shown in Chapter 2.5.3, inward-propagating gravity waves excited with low frequency at the periphery of sufficiently intense TCs (maximum wind > 50 m s^{-1}) can be absorbed at critical radii where their frequency is Doppler shifted to the Brunt-Vaisala frequency (Willoughby 1978). Although the wave pattern resulting from absorption near

the radius of maximum wind suggests an eye, it is difficult to relate this phenomenon dynamically to eye formation. Some observational evidence supports inward-propagating waves, and their interaction with the axisymmetric vortex at critical loci seems plausible (Willoughby *et al.* 1984), but they are probably not the spiral bands that one sees on radar.

Although it is possible that inertial instability (Xu 1983) plays a role in band formation, observations indicate that the necessary conditions are rarely met in real TCs (Black and Anthes 1971). Other hydrodynamic instabilities are, however, potential sources of asymmetric motions (Emanuel 1984). The wind profile inside the eye (e.g., Fig. 2.4) is often "U-shaped" in the sense that the wind increases outward more rapidly than linearly with radius. The strong cyclonic shear just inside the eyewall results in a local maximum of absolute vorticity, so that the profile may be barotropically unstable. Guinn and Schubert (1993a) hypothesize that this instability may explain the "polygonal eyewalls" described by Lewis and Hawkins (1982). It may also explain intense mesoscale vortices in the eyewalls of Hurricanes Hugo of 1989 (Black and Marks 1991) and Andrew of 1992.

Motion of the vortex through its surroundings may cause one kind of stationary band (Willoughby *et al.* 1984). In the vortex core, air remains in the circulation for many orbits of the center; in the outer envelope, the air passes through the circulation in less than the time required for a single orbit. A frequently observed stationary spiral called the principal band (Fig. 2.14) lies along a convergent streamline asymptote (Sherman 1956) that spirals into the core from the envelope. This same feature appears in Fig. 2.2, where it connects the core of the composite Australian TC with the monsoon trough. A TC advected by middle-level steering with westerly shear will move eastward through surrounding air at low levels. Thus, the principal band may be a "bow wave" (Beer and Giannini 1980) due to displacement of the environmental air on the eastern side of the vortex. Its predominant azimuthal wavenumber is one, and dynamically it may be more like a convective ring than a gravity wave (Willoughby *et al.* 1984). Although observations of Hurricanes Alicia (Willoughby 1990a) suggest that convective rings can form by detachment from the inward sides of the principal band, coalescence of higher wavenumber bands, as happened in Hurricanes Gilbert and Danny, is also a common mode of formation.

In addition to the squall-line or gravity-wave spirals, some asymmetries may be Rossby waves that depend upon the outward decrease in relative vorticity from the TC center (MacDonald 1968). One example that is clearly a Rossby wave is the "beta gyre" asymmetry (Fiorino and Elsberry 1989) that is responsible for poleward and westward vortex propagation on a beta plane (Fig. 2.16). This structure has a horizontal scale of ~1000 km, which is comparable with that of the vortex. It appears as a wavenumber 1 streamfunction dipole with an anticyclonic gyre poleward and east of the center and a cyclonic gyre equatorward and west of the center (see Fig. 4.32). As shown in Chapter 4.3.1.2, a more or less uniform current flowing across the center of the vortex between the gyres advects the vortex westward and poleward (Holland 1983b, 1984) and spins the vortex down through the Coriolis torque (Holland 1983a). The Rossby wave dynamics are a balance between advection of the asymmetric vorticity around the vortex by the axisymmetric swirling, and advection of the axisymmetric vorticity by the asymmetric radial flow. Although the beta gyres may represent a normal mode(s) of the vortex (Willoughby 1990c), this interpretation is controversial (Peng and Williams 1991; Weber and Smith 1993).

Higher wavenumber Rossby waves probably exist as well. Shapiro and Montgomery (1993) have formulated an "asymmetric balance" approximation that is clearly valid for wavenumber 1, but breaks down for the higher wavenumbers near the vortex center. The center boundary condition requires ψ_n, the streamfunction for the wavenumber n asymmetry, to approach $r^n e^{-in\lambda}$ near the center. Thus, only the wavenumber 1 rotational asymmetry has any flow across the center. For $n \geq 2$, both ψ_n and its gradient are zero at the origin. A second effect that reduces ψ_n for $n \geq 2$ is vortex symmeterization as the radial gradient of axisymmetric angular velocity distorts vorticity-conserving disturbances to

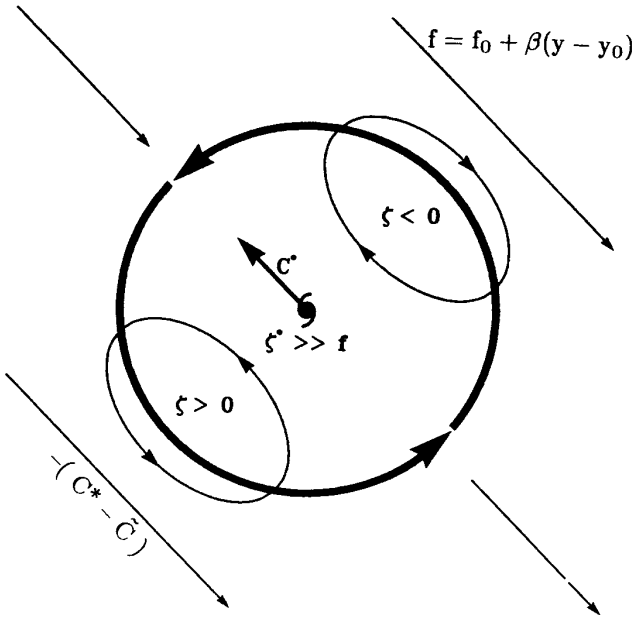

Fig. 2.16 Wavenumber 1 asymmetry in a Northern Hemisphere cyclone propagating westward and poleward with velocity c on a beta plane. Cyclonic vorticity is positive. The heavy circle represents the mean circulation; the lighter ellipses represent the asymmetric perturbation gyres; and the straight arrows represent the relative motion of the cyclone through its environment (Willoughby 1990c).

higher radial wavenumbers, and thus reduces their amplitudes (Carr and Williams 1989; see Fig. 4.34). The center boundary condition and symmeterization are two reasons why balanced asymmetries with wavenumber ≥ 2 are less important in the core than outside.

2.4 ENVIRONMENTAL FORCING

Thermodynamic forcing by the underlying sea and dynamic forcing from the surrounding air seem to control hurricane evolution. Sometimes, sea-surface temperature (SST) clearly modulates intensity changes (Perlroth 1962, 1967). At other times, synoptic-scale atmospheric interactions modulate intensity (e. g., Ramage 1974). A general consensus exists that small vertical shear of the environmental wind and lateral eddy imports of angular momentum are favorable to tropical cyclone intensification. Although the potential maximum intensity is determined by the temperature of the underlying sea (see Chapter 2.4.3), it is the atmospheric forcing that determines how closely the actual intensity approaches the potential intensity (Merrill 1988b).

2.4.1 Atmospheric forcing

The inhibiting effect of vertical shear in the environment on TC intensification is well known from climatology (Palmen 1956; Gray 1968) and forecasting experience (Clark 1983; Case and Gerrish 1984; Pasch and Avila 1992). The conventional wisdom is that strong relative winds in a sheared environment "ventilate" the vortex core (Simpson and Riehl 1958) and "decouple" the upper-tropospheric warm anomaly from the lower-tropospheric latent heat convergence. The appearance of the low-level circulation outside the TC's central dense overcast in satellite imagery is universally recognized as a symptom of shear and as an indication of nonintensification or weakening (Dvorak 1984). Nevertheless, the detailed dynamics of a vortex in shear has been the topic of surprisingly little study, probably because the effect is a reliable basis for practical forecasting, but it is difficult to model.

In contrast, the positive effect of eddy momentum imports at upper levels has received extensive study. Modeling studies with composite initial conditions (Challa and Pfeffer 1990; Pfeffer and Challa 1992) show that eddy momentum fluxes can spin up a TC even when other conditions are neutral or unfavorable. Indeed, Montgomery and Farrell (1993) showed theoretically that momentum imports can form a TC in an atmosphere with had no convective buoyancy. In this study, the atmosphere was neutral in the sense that condensation provided the energy to move the air from the surface to the tropopause, but had no excess buoyancy. Momentum forcing sustained the upper divergence that caused the vertical motion. Case studies also show that eddy momentum fluxes sometimes modulate intensity changes through initiation of outer eyewalls (Molinari and Vollaro 1989, 1990). Statistical analysis of Atlantic hurricanes and tropical storms during the 1989-1991 seasons reveals a clear relationship between angular momentum convergences and intensification, but only after the effects of shear and SST variations are accounted for (DeMaria *et al.* 1993).

Extensive composite analysis of Atlantic hurricanes (Merrill 1988a) appears not to confirm this relationship between intensification and eddy momentum fluxes. The composites do show that intensifying hurricanes have unrestricted outflows that are organized into jets that decelerate as they diverge from the vortex center (Fig. 2.17). On the other hand, nonintensifying hurricanes have unidirectional flow across the center and closed streamlines that merge back into the vortex. The radial outflow is stronger in intensifying hurricanes. Paradoxically, the tangential anticyclonic flow is weaker than in nonintensifying ones (Merrill 1988b). Although convective addition of cyclonic momentum to the outflow (Lee 1984) may be an explanation, a more likely reason for the weaker anticyclone is eddy momentum imports not resolved in the composite analysis.

As indicated in Fig. 2.3, the secondary circulation response to momentum and heat sources are very different. Holland and Merrill (1984) show a convective heat source forces essentially vertical motion that extends through the depth of the troposphere (Fig. 2.18a). In a weak TC, a mechanism by which environmental convection can affect the core is inward propagating low-level surges of moisture and convection that cause intensification when they reach the vortex center (Molinari and Skubis 1985). Because the *mature* TC core has a large radial gradient of angular momentum in the lower and midtroposphere, environmental convection can not influence the vortex core directly. On the other hand, upper-tropospheric momentum sources can influence the core directly (Fig. 2.18b). Whereas large inertial stability in the lower troposphere protects the mature TC core from direct influence by momentum sources, the inertial stability in the upper troposphere is so small that a momentum source can induce an outflow jet with large radial extent just below the tropopause. The eyewall updraft then joins the entrance into the jet so that the exhaust outflow is unrestricted. The important difference between heat and momentum

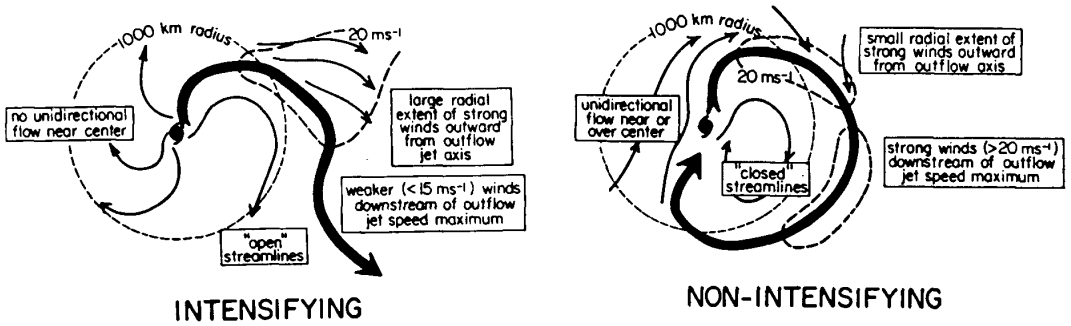

Fig. 2.17 Differences between the outflow and upper-level asymmetries of intensifying and nonintensifying hurricanes (Merrill 1988b).

sources is that the diabatically-induced updraft must have its roots in the inertially stiff lower troposphere, but the outflow jet due to a momentum-flux convergence can be confined to the inertially labile upper troposphere. Momentum forcing does not spin the vortex up directly. It makes the exhaust flow stronger and reduces local compensating subsidence in the core, thus cooling the upper troposphere and destabilizing the sounding. The cooler upper troposphere leads to less thermal-wind shear and a weaker upper anticyclone.

The environmental flows that favor intensification, and presumably inward eddy momentum fluxes, usually involve interaction with a synoptic-scale cyclonic feature (Fig. 2.19), such as a midlatitude trough or TUTT (Tropical Upper Tropospheric Trough) cell (Koteswaram 1967; Ramage 1974; Sadler 1976). The outflow is commonly organized into jets. In a Fourier analysis that resolves the radial flow into azimuthal wavenumber components, only the axisymmetric component can sustain a net outflow. The wavenumber ≥ 1 components concentrate the outflow into the jets that appear in satellite images, but their real dynamic effect is the momentum convergence that induces the wavenumber 0 outflow.

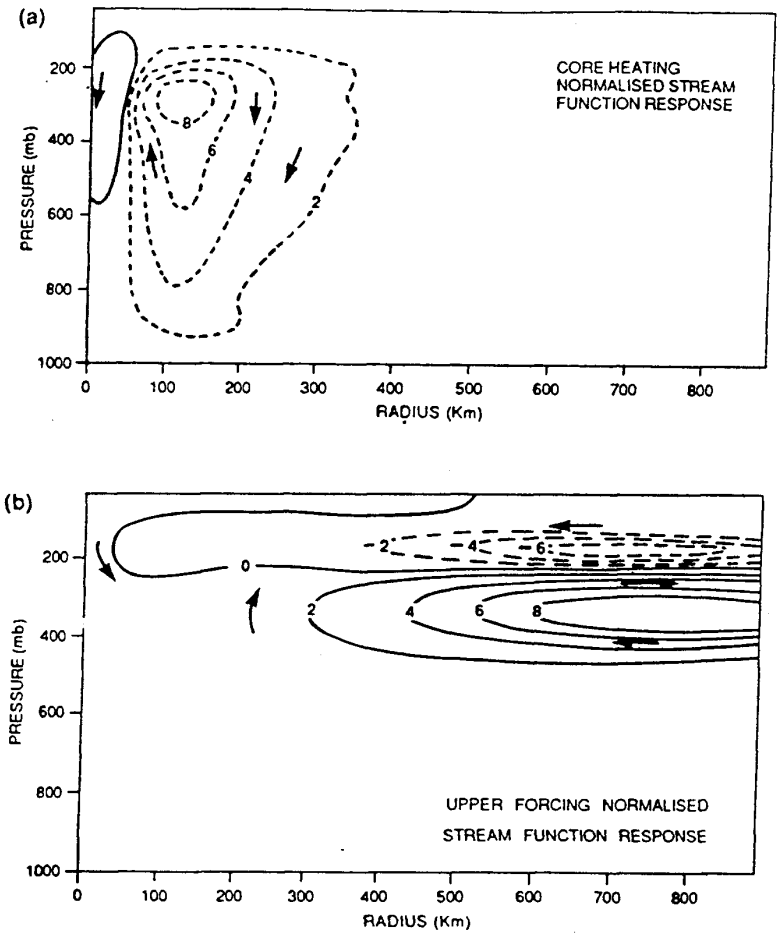

Fig. 2.18 Normalized streamfunction fields showing the secondary circulation induced on a balanced vortex (*a*) by heating in the vortex core, and (*b*) by a cyclonic momentum source in the upper-tropospheric environment (Holland and Merrill 1984).

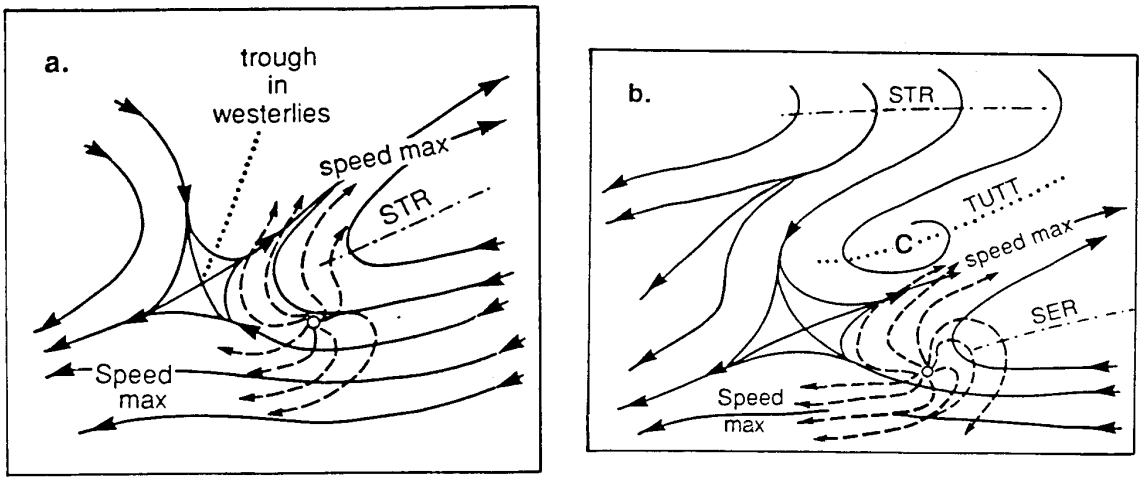

Fig. 2.19 Two synoptic models of upper-level environmental interactions that favor tropical cyclone intensification: (a) a trough in the westerlies and (b) a TUTT cell. STR denotes the SubTropical Ridge, SER the SubEquatorial Ridge, and TUTT the Tropical Upper--Tropospheric Trough (Sadler 1978).

2.4.2 Boundary layer

To a first approximation, the axisymmetric turbulent forcings F_{uB}, F_{vB}, $F_{\theta B}$, and F_{qB} of the axisymmetric radial wind (u_B), tangential wind (v_B), potential temperature (θ_B), and absolute humidity (q_B) at the sea surface can be modeled with the bulk aerodynamic formulae (e. g., Roll 1965), and the fluxes through the top of the boundary layer at $z = H_B$ can be neglected:

$$F_{uB} = -C_D \frac{v_B u_B}{H_B}, \tag{2.10.1}$$

$$F_{vB} = -C_D \frac{v_B^2}{H_B}, \tag{2.10.2}$$

$$F_{\theta B} = -C_\theta \frac{v_B(\theta_B - \theta_c)}{H_B}, \tag{2.10.3}$$

$$F_{qB} = -C_H \frac{v_B(q_B - q_c)}{H_B}, \tag{2.10.4}$$

where C_D, C_θ, and C_H - 1-3 x 10^{-3} are the bulk aerodynamic transfer coefficients, which may be different for each variable and may be functions of windspeed (e. g., Moss and Rosenthal 1975). θ_c and q_c are the potential temperature and saturation mixing ratio at the sea-surface temperature. The motion of the sea surface is assumed to be negligible compared with the wind speed and $u_B << v_B$ so that $(u_B^2 + v_B^2)^{1/2}$ - v_B. The conventional wisdom is that the inflow is approximately isothermal and maintains a relative humidity of 80%-90%, so that diabatic expansion increases θ_B and q_B.

Substitution of F_{vB} from (2.10.2) into the axisymmetric tangential momentum equation (2.14.1b) produces an expression for the radial flow in the boundary layer

$$u_B = -\frac{C_D v_B^2}{H_B\left(\frac{\partial v_B}{\partial r} + \frac{v_B}{r} + f_0\right)}. \tag{2.11}$$

Equation (2.11) embodies the "momentum integral" concept of first-order balance between inward advection of angular momentum and frictional loss to the sea in the TC boundary layer (Smith 1968; Leslie and Smith 1970). The isallobaric term, vertical advection, and horizontal eddy transports have been neglected. This expression explains some aspects of the distribution of convection in hurricanes. At large radius where the Rossby number $R_0 = v_B/f_0r << 1$, f_0 predominates over the relative vorticity in the denominator. The inward increase of frictional stress with increasing v_B causes inflow to increase downstream. Over much of the area, acceleration overwhelms confluence, so that the inflow is horizontally divergent and draws air downward from the overlying atmosphere, and thus forms a clear outer moat (Frank 1977a). Inside the 100-200 km radius where $R_0 > 1$, the relative vorticity predominates over f_0 in the denominator. Under these conditions, the inflow is proportional to rv_B because the vorticity in the denominator tends to be proportional v_Br^{-1}, while the stress in the numerator is proportional to v_B^2. Thus, the inflow is convergent because it is both confluent and decelerates downstream. The radius where $R_0 \sim 1$, which is typically 100-300 km, encompasses the convective areas of most TCs (Willoughby *et al.* 1984).

As the inflow passes through the radius of maximum wind, $\partial v_B/\partial r$ changes sign from negative to positive, so that the denominator in (2.11) increases by a factor of ~ 4 to produce an abrupt deceleration of the inflow and a sharp convergence beneath the eyewall updraft. If the stress depended linearly on the wind, as happens in Ekman pumping, the maximum convergence would lie at the vortex center where the vorticity is maximum. It is because the stress depends quadratically on v_B that the convergence at the vortex center is zero and the strongest convergence lies near the radius of maximum winds (Eliassen 1971). Theoretical analysis of asymmetric friction (Shapiro 1983) shows that in slowly moving (speed $\leq$ 5 m s^{-1}) hurricanes, maximum convergence tends to localize convection in the right-front quadrant of the eyewall. In more rapidly moving hurricanes, the strongest convergence moves more toward the front of the eyewall. Observations in hurricanes Frederic (Powell 1982) and Allen seem to support these results, but a recent study of Hurricanes Alicia and Elena does not (Burpee and Black 1989).

Based upon aircraft measurements (Moss and Merceret 1976; Moss 1978), the hurricane boundary layer is well mixed and dominated by mechanical turbulence. Enthalpy, specific humidity, and momentum are nearly constant over the 650 m depth of the boundary layer. Generation of turbulent kinetic energy in the Prandtl (constant stress) layer balances dissipation integrated over the boundary layer as a whole, and buoyancy production is small. The stress seems to vanish at the top of the boundary layer in these observations. Nevertheless, composite analyses (Frank 1977b,c), modeling results (Anthes and Chang 1978), and one case study (Riehl 1981) raise doubts about the assumption of zero vertical fluxes at the top of the boundary layer. Under the stratiform central dense overcast, the air just above the boundary layer is warm, relatively dry mesoscale downdraft air that swirls about the center with nearly the gradient-wind velocity. Entrainment mixing would thus warm and dry the boundary layer and accelerate its rotation. Given the relatively small air-sea temperature difference (1°-2°C), entrainment of potentially warm air from above may be a more important source of sensible heat than turbulent transfer from the sea. Entrainment mixing may be the mechanism that keeps the inflow nearly isothermal and undersaturated (Malkus and Riehl 1960) against adiabatic expansion and moistening by evaporation from the sea. The drying also enhances the latent heat flux that fuels the vortex as a whole. The downward momentum flux due to entrainment and convective downdrafts would counteract the frictional torque and reduce the inflow velocity, but probably only a little since the swirling wind integrated over the depth of the boundary layer is only slightly subgradient.

2.4.3 Sea-surface temperature and intensity

Since the tropical ocean is the energy source for TCs, it is reasonable to suppose that warmer water can support stronger cyclones. This supposition has been explored

through thermodynamic calculation and comparison between observed intensity and SST. Miller (1958) assumed a sounding in an eye that was surrounded by an eyewall in which the sounding was a moist adiabat that originated at the surface with temperature equal to the SST and 85% relative humidity. The air in the eye began its descent from the top of the vortex as eyewall air. It descended without dilution to 10 km altitude and then was diluted with eyewall air following a quadratic empirical formula tuned to match relative humidities in the eyes of observed TCs. The resulting variation of MSLP with SST (Fig. 2.20a) was realistic. An important unanswered question was: how does the eye draw moisture from the eyewall without also acquiring angular momentum? An SST of 27°C corresponded to a minimal hurricane (MSLP ~ 980 mb). An SST of 31°C, which is at the high end of the observed range, corresponded to the most intense hurricanes (MSLP < 900 mb). Comparison between observed MSLPs at maximum intensity and potential MSLP calculated from analyzed SSTs yielded agreement in five of eight contemporary hurricanes and potential MSLP 15-20 mb lower than observed in the others.

On the observational side, Merrill (1988b) compared maximum surface winds of Atlantic hurricanes with climatological SSTs at the hurricane position (Fig. 2.20a). The upper bound defined by the greatest wind speed for each SST was qualitatively similar to Miller's, but the SSTs that correspond to a given MSLP were 1-2°C cooler, e. g., 900 mb MSLP corresponded to 29°C in Merrill's observations, but 31°C in Miller's model. Comparison between theoretical and observational studies of this kind is difficult because the former generally predicts minimum sea-level pressure and the latter predicts maximum wind. Even allowing for the inaccuracies of pressure-wind relations, Miller's and Merrill's results clearly differ, perhaps because Merrill's extreme intensities represent a coincidence of favorable conditions, which may include warm SST anomalies in addition to favorable atmospheric forcing.

A logical extension of the thermodynamic approach (Emanuel 1986) treats the secondary circulation as a Carnot cycle: diabatic, isothermal inflow; moist adiabatic ascent and outflow; and radiatively-driven descent in the environment to close the cycle. This study parameterizes the dynamics in terms of the thermodynamics by exploitation of gradient balance to express angular momentum as a function of moist enthalpy. Although the secondary circulation has some unrealistic properties, e.g., ascent throughout the vortex, including the eye, it seems to capture the essence of the thermodynamic problem. The lowest attainable surface pressure increases with thermodynamic efficiency $\epsilon = (T_C - T_O)/T_C$, where T_C is the near-surface inflow temperature and T_O is the temperature of the outflow near tropopause level. For extreme intensities, the potential minimum pressures agree with Miller's in that a 900 mb TC would require a SST of ~31°C if T_O were -75°C (Fig. 2.20a). For lower SSTs, the predicted intensities at the same T_O are greater than in either Miller's model or Merrill's observations. With fixed T_O, the potential minimum pressure declines about 10 mb for every 1°C increase in SST in the range near 30°C, and similarly for every 5°C decrease in tropopause temperature. The potential intensities calculated from this scheme with climatological SST and tropopause temperature for September seem to agree with the most extreme intensities observed (Fig. 2.20b). Clearly, a warm ocean and a cold tropopause are necessary, although by no means sufficient, conditions of extreme TC intensity. At high SSTs (> 40°C), the theoretical calculation breaks down to predict "hypercanes," in which the minimum sea level pressure becomes equal to the vapor pressure of water at the SST (Emanuel 1988).

DeMaria and Kaplan (1994) elaborate Merrill's approach by use of actual SSTs for a 31-year sample of North Atlantic TCs. Their curve predicts greater intensity than Merrill's at SST > 28.5°C and weaker intensities for lower SST (Fig. 2.20a). Comparison between the intensities of individual TCs with the maximum shows that only one in five reaches 80% of its potential, and the average TC reaches a little more than half its potential maximum wind. Many of the TCs that approach their potential intensities do so by motion over cooler water rather than by intensification. Comparison of DeMaria and Kaplan's potential intensity with Emanuel's at tropopause temperatures of -70°, -75°, and

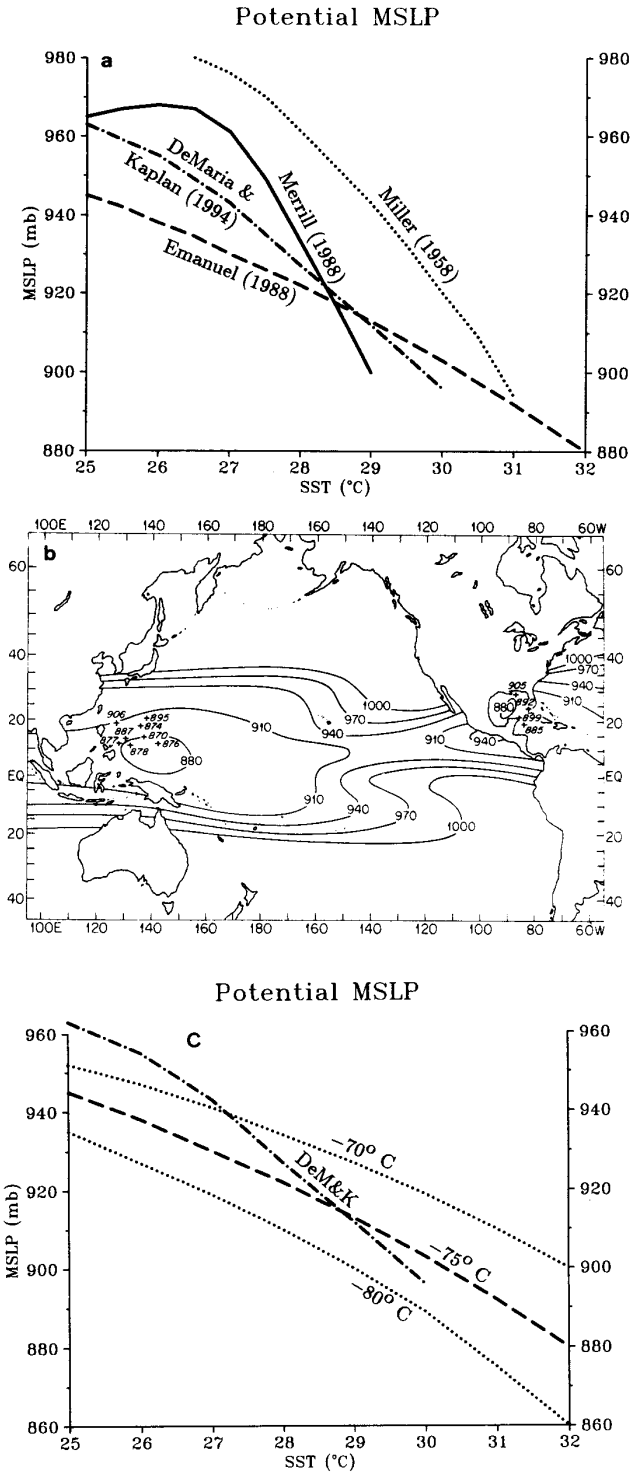

Fig. 2.20 (a) Potential minimum sea-level pressure in tropical cyclones as a function of sea-surface temperature from observational studies by Merrill (1988b) and DeMaria and Kaplan (1994) and thermodynamic studies by Miller (1958) and Emanuel (1986). The curve from Emanuel's results uses -75°C outflow temperature. (*b*) Extreme minimum sea-level pressures observed in tropical cyclones plotted over a map of potential minimum pressures calculated from climatological data for September. (*c*) Comparison of DeMaria and Kaplan's empirical curve with Emanuel's results for outflow temperatures of -70°, -75°, and -80°C.

-80°C (Fig. 2.20c) shows that the empirical intensities at lower SSTs coincide with a warmer (lower altitude) tropopause, and higher SSTs with a cooler (higher) tropopause, as one might expect from the rise of tropopause height toward the equator. Thus, the climatological negative correlation between T_c and T_o enhances the effect of a warmer sea to produce a potential MSLP fall of 15 mb per °C compared with 10 mb per °C in Emanuel's model with fixed T_o.

Holliday and Thompson (1979) find that 75% of the typhoons that reach MSLP < 920 mb do so through rapid deepening ($\geq$ 42 mb in 24 h). All cases of rapid deepening occurred over water warmer than 28°C and oceanic mixed layers deeper than 30 m. Since most typhoons encounter equally favorable oceanographic conditions, but do not deepen rapidly, this observation argues that some other factor, possibly interaction with a TUTT cell, is essential to the onset of rapid deepening. Evans (1993) examined a 20-year record of TC intensity and monthly mean SST in the Atlantic, Pacific, and Indian Oceans. She concluded that while SST may define the potential intensity, it is not the most important factor in intensification. Nonetheless, the strongest TCs with v_m > 70 m s^{-1} occurred only over SST > 28°C. Evans argued that a discontinuous increase in potential intensity at that threshold fitted the observations as well as the curves in Fig. 2.20a. The lack of observations of $v_m \geq$ 90 m s^{-1} supports this view.

These data contain no observations of extreme intensities at SST > 30°C. One possible explanation is the convection albedo thermostat (Ramanathan and Collins 1991) in which SSTs approaching 31°C set off convection that spreads a veil of cirrus that shields the surface from insolation. Thus, the warmest sea might be the site of monsoon-trough convection and possibly of tropical cyclogenesis, but it would not be a place where mature TCs would reach their maximum intensity. Another plausible explanation is that cooling by evaporation of blowing spray at extreme wind speeds may inhibit intensification. Shipboard and rawinsonde measurements in tropical storms Tess and Skip of 1988 at windspeeds up to 25 m s^{-1} support the existence of this cooling (Korolev *et al.* 1990), and boundary layer modeling based upon parameterized spray evaporation shows a significant effect (Fairall *et al.* 1995; Kepert 1995).

2.2.4 Landfall

As a tropical cyclone approaches land, the outer winds begin to be modified. Intense convection tends to form ahead of the TC center and to its right in the frictional convergence where onshore winds reach the coast (Parrish *et al.* 1982; Burpee and Black 1989). This asymmetric heating tends to induce a track acceleration toward the enhanced convection by forcing vortex asymmetries as described theoretically by Willoughby (1992). In Atlantic hurricanes, weakening just before landfall often results from eyewall replacements (Willoughby 1990a). Although the sample is admittedly biased toward landfalling cases, the frequent coincidence of outer eyewalls with landfall makes it seem that they are induced by proximity to land.

Once a TC has passed onshore, increased roughness leads to an immediate reduction of surface winds (e. g., Powell 1982, 1987). Nevertheless, the primary mechanism that weakens the vortex as a whole is not friction, but loss of the oceanic heat source (Bergeron 1954; Hubert 1955; Miller 1964). Over land, the frictional inflow becomes moist adiabatic rather than nearly isothermal and the low-level air spiralling toward the center cools more rapidly. This process occurs even over wet land surfaces (such as the Florida Everglades or North Australia during the rainy season) because it is cooling of the underlying surface, not the absence of water, that interferes with latent heat transfer (Tuleya 1994). Heat conduction through the solid earth is much slower than vertical mixing in the sea, and the earth's heat capacity is smaller. Thus, in contrast with a warm, fairly deep oceanic mixed layer, the land surface cools so quickly that it can not continue to supply heat to the TC. Eventually, the core expands in response to the weakened convective forcing.

Although friction saps the surface winds virtually from the shoreline, convection can bring strong winds to the surface inland (Fujita 1993; Wakimoto and Black 1994). Sustained wind and gustiness at a particular site is a strong function of topography and the small-scale roughness of the surrounding surface (Padya 1975; see Chapter 6.8.2). Rapidly translating TCs, such as Hurricanes Hugo of 1989 (Powell and Black 1990) or Andrew of 1992, present a greater inland wind hazard because they have less time to weaken after they cross the coast. As described in Chapter 6.7.3, rapidly filling TCs with strong vertical shear at the top of the boundary layer often produce tornadoes, predominantly in their northeast quadrants (Novlan and Gray 1974).

Apart from boundary-layer spindown and the collapse of the eyewall wind maximum, the surviving residual circulation is often not too different from the original TC. The TC circulation above the boundary layer is in large measure isolated from surface friction and may persist for days as it continues to exhibit a characteristic TC appearance on radar and to produce substantial rainfall (Bluestein and Hazen 1989). Indeed, inland rainfall and flooding, particularly in the mountains, is an important part of the threat that TCs pose to life and property (Schwartz 1970; Bosart and Carr 1978). If the mid-tropospheric remnants return to a warm ocean, a TC may redevelop (Brand and Blelloch 1973; McBride and Keenan 1982). As in the case of initial cyclogenesis, the mechanism by which the warm-core midlevel circulation builds downward to the surface (e. g., Menard and Fritsch 1989) remains unknown.

Special circumstances apply when TC landfall is on a mountainous coastline. For example, weakening of Hurricane Allen was correlated with mountains in the circulation (Hawkins 1983). Track and intensity fluctuations were also documented in other case studies of Atlantic hurricanes (Willoughby *et al.* 1984; Willoughby 1990a). Typhoons approaching the Philippines and Taiwan also tend to weaken (Brand and Blelloch 1973, 1974). Track changes upstream of mountains are still a topic of research. Whereas Brand and Blelloch (1974) suggested an acceleration began far upstream of Taiwan, Yeh and Elsberry (1993) provide evidence that the translation speed increase is associated with the large-scale environmental flow. Yeh and Elsberry provide observational and modelling evidence for the upstream track deflection to first be toward the north (south) as expected for a northern (southern) TC embedded in a "blocked" flow around the Taiwan orography. However, severe modification of the interior flow (tangential winds > 15 m s^{-1}) as the TC interacts with orography then leads to a south (north) track deflection that can significantly change the landfall point. The magnitude of the latter track deflection is larger for slower moving and weaker typhoons. Zehnder (1993) suggests the Sierra Madre of Mexico induces track deflections toward higher values along the gradient of potential vorticity due to gradients of topography. These deflections are to the left of the track, south for TCs approaching the mountains from the east and north for those approaching from the west.

2.4.5 Extratropical transformation

As TCs move out of the tropics, the environmental forcing changes because the synoptic-scale environmental winds become stronger, the ocean surface is cooler, and horizontal temperature gradients outside the vortex increase. The stronger environmental winds in midlatitudes lead to acceleration of the TC translation and a greater asymmetry between the hazardous semicircle (where the TC and environmental winds add) and navigable semicircle (where they subtract). Since recurvature out of the tropics usually takes place along the western shore of an ocean, a TC whose center remains offshore projects the weaker winds of the navigable semicircle ashore while the stronger winds of the hazardous semicircle remain at sea. In such situations, coastal locations experience the hazardous semicircle only when the center passes onshore. Stretches of coastline that trend east-west, such as Cape Hatteras and Long Island to Cape Cod in North America and the Japanese coast west of Tokyo Bay, are particularly vulnerable to this kind of landfall. The 1938 New England Hurricane (Allen 1976) was a notable example in which great damage

and loss of life occurred through accelerated translation of the TC rather than strengthening of the swirling wind.

The reduced oceanic heat source in midlatitudes leads to generally weaker convection. Once a TC has passed the poleward boundary of the warm western ocean boundary currents (such as the Gulf Stream or the Kuroshio Current), it loses the sharply peaked wind profiles that characterize the most intense TCs in the deep tropics. The flat wind profile, which is part of the general expansion of the TC circulation with age and poleward propagation (Merrill 1984), may lead to an overestimation of the maximum wind from the wind pressure relationships in Chapter 2.2.3.

The transition of Hurricane Gloria of 1985 as it tracked northward along the east coast of North America illustrates extratropical transition in a largely barotropic environment (Willoughby 1990a). Gloria weakened as a result of an eyewall cycle while still over warm water. The profile of the TC-relative wind that resulted was flat with a constant value of ~ 40 m s^{-1} out to > 150 km from the center. The hurricane never recovered a peaked profile before it encountered cool water poleward of 35°N. The wind profile as Gloria approached landfall on Long Island east of New York City was much like that in Hurricane Gilbert after it passed over the shallow oceanic mixed layer in the Bay of Campeche (Fig. 2.11b). Indeed, these "flat-forty" profiles with 40 m s^{-1} winds extending more than 100 km from the center seem to characterize large, formerly intense TCs that have weakened for whatever reason.

Although TC convection is less vigorous over cool water, frictional convergence in the boundary layer continues to organize convection into bands and rings so that the TC maintains its characteristic appearance on radar far into the weakening process. As the organized convection dissipates, strong isolated convective "supercells" may consume the last of the convective energy, as happened in Hurricane Gert of 1981 (Willoughby *et al.* 1984). In contrast to conditions over warm water, where the convection carries most of the mass flux in the vertical branch of the secondary circulation, so little convective ascent occurs over cool water that the air converged in the friction layer rises only to the top of the boundary layer and flows outward in the lower troposphere (Willoughby 1979). Frictional inflow and adiabatic ascent thus weakens the swirling wind and cools the vortex core in the boundary layer, and the midlevel circulation is decoupled from surface friction. This change in structure may explain forecasting experience that recognizable circulations may persist for days over cool extratropical oceans.

Extratropical transition in the strict sense is the change from an axisymmetric, warm core TC to an asymmetric, baroclinic extratropical cyclone. The large spatial scale of most poleward-moving TCs and their passage through dense mid-latitude observation networks make extratropical transition a good subject for case studies that employ the tools of conventional synoptic analysis. As Hurricane Hazel of (1954) was transformed into an intense extratropical cyclone over eastern North America (Palmen 1958), it generated ~ 2 x 10^{10} kJ of kinetic energy. This quantity was between half and a quarter of the frictional dissipation in the westerlies of the entire Northern Hemisphere during the same period. The mechanism of baroclinic energy generation was conversion from available potential energy through downgradient flow or, equivalently, through ascent of warm air and descent of cool air. Since the reservoir of available potential energy was so large and substantial heating by condensation occurred in the warm air, the kinetic energy increase did not cause a decrease of available potential energy. Most of the newly generated kinetic energy was exported to Hazel's environment.

In Tropical Storm Agnes of 1972 (DiMego and Bosart 1982a,b), the kinetic energy generation, again primarily by down-gradient flow, was only 40% of that in Hazel. Convective ascent in the warm air was also important. In contrast with Hazel, the kinetic energy generation primarily increased the kinetic energy locally and balanced dissipation with little export to the environment. Agnes redeveloped as a result of convection in the convergence between warm, moist air advected inland ahead of the TC and cooler air over the Appalachian mountains (Bosart and Dean 1991). In the area along the front of the

mountains, diabatic heating, thermal wind advection, and upper vorticity advection combined to create a new circulation center as Agnes' original circulation passed over Long Island and dissipated. This process appears to be an example of complex extratropical transition as occurred in Typhoons Doris of 1966 and Winnie of 1966 (Sekioka 1970). Both typhoons drew fronts into their circulations and induced new extratropical cyclones that became distinct from the original TC. This process contrasts with typhoons that did not capture the fronts and dissipated without redevelopment.

Brand and Guard (1979) examined 16 recurving western North Pacific TCs in 1971 that continued to have high winds and seas for as long as five days after recurvature. On the average, the maximum wind decreased and speed of translation increased after recurvature. The radius of 15 m s^{-1} wind increased slowly for the first 3 days and then decreased. Six of the TC remnants reached the Aleutians or North America as recognizable extratropical cyclones.

2.5 DYNAMICS

2.5.1 Governing equations

This section explores the physical and mathematical interpretation of the observations presented in the previous sections. As with other atmospheric motions, tropical cyclones are described using Newton's second law, augmented by conservation laws for mass, thermodynamic energy, and water vapor. Although virtually all numerical modeling of TCs has been carried out in coordinates fixed to the Earth, it is convenient for this discussion to express the governing equations in a translating system that tracks the moving vortex. The origin of the coordinates coincides with the axis of rotation. It has a position vector $r_0(t)$, moves with velocity c, and may have an acceleration $\dot{\mathbf{c}}$. In translating, log-pressure coordinates (e. g., Holton 1992) on a rotating spherical Earth, the governing equations have the form

$$\frac{\partial \mathbf{v}}{\partial t}+\mathbf{v}\cdot\nabla\mathbf{v}+w\frac{\partial \mathbf{v}}{\partial z}+f\mathbf{k}\times\mathbf{v}+\nabla\phi=-[\dot{\mathbf{c}}+f\mathbf{k}\times(\mathbf{c}-\tilde{\mathbf{c}})]+\mathbf{F}_v, \tag{2.12.1}$$

$$\frac{\partial w}{\partial t}+\mathbf{v}\cdot\nabla w+w\frac{\partial w}{\partial z}-g\frac{\theta-\theta_0}{\theta_0}+\frac{\partial \phi}{\partial z}=\mathrm{F}_w, \tag{2.12.2}$$

$$\nabla\cdot\mathbf{v}+\frac{\partial w}{\partial z}-\frac{w}{H}=0, \tag{2.12.3}$$

$$\frac{1}{\theta_0}\left[\frac{\partial \theta}{\partial t}+\mathbf{v}\cdot\nabla\theta\right]+w\frac{N^2}{g}=-\frac{1}{\theta_0}\mathbf{v}\cdot\nabla\tilde{\theta}+\frac{Q}{c_pT_0}+\mathrm{F}_\theta, \tag{2.12.4}$$

$$\frac{\partial q}{\partial t}+\mathbf{v}\cdot\nabla q+w\frac{\partial q}{\partial z}=-\mathbf{v}\cdot\nabla\tilde{q}+E-C+\mathrm{F}_q. \tag{2.12.5}$$

Here, t is time, $\mathbf{r} = (x, y)$ is horizontal position relative to the vortex center, $z = -H \ln (p/P)$ is the log-pressure vertical coordinate, where H is the scale height, p is pressure and $P = 1000$ mb. In the log-pressure system, v is the wind in the plane of the z surfaces, w is the wind normal to the z surfaces, positive upward, and ∇ is the two-dimensional gradient operator on the z surfaces. $2\,\Omega_E \sin\gamma = f$ is the Coriolis parameter at latitude γ on the Earth rotating with angular velocity Ω_E, and k is a unit vector pointing in the z direction. T and θ are the temperature and potential temperature. $T_0(z)$, $\theta_0(z)$ and $\rho_0(z)$ are the reference temperature, potential temperature, and density in the undisturbed atmosphere, such that $H^{-1} = \rho_0^{-1}\partial\rho_0/\partial z = g/RT_0$, where g is the gravitational acceleration and R is the gas constant for dry air. $N^2 = g/\theta_0^{-1}(\partial\theta_0/\partial z)$ is the square of the Brunt-Vaisala frequency. For simplicity, $T_0, \theta_0, \rho_0, N^2$ and H are treated as functions of z alone, and the

intersections of z isolines with the sea surface in the region of low pressure near the TC center are disregarded. Q is the heating rate, which includes both latent heat release and radiation, c_p is the specific heat of dry air at constant pressure, and q is the specific humidity. E is the evaporation, C is condensation, and $\mathbf{F}_v$, F_μ, F_θ, and F_q represent the effects of molecular and turbulent diffusion of horizontal and vertical momentum, heat, and water vapor.

The environmental flow $\tilde{\mathbf{c}}$ is assumed to be in geostrophic balance with the environmental geopotential perturbation $\tilde{\phi}$ so that $f\,\mathbf{k} \times \tilde{\mathbf{c}} = \tilde{\phi}$. The mass field in the environment is hydrostatic, so that the potential temperature distribution in a baroclinic environment is given by the thermal wind relation $(\nabla\theta)/\theta_0 = (f/g)\,\mathbf{k} \times (\partial\tilde{\mathbf{c}}/\partial z)$. The terms associated with vortex motion that appear on the right side of (2.12.1) are: the actual acceleration of the coordinate system, the Coriolis acceleration due to the coordinate system translation, and the environmental pressure gradient, represented as a geostrophic wind. Only in the special case of constant vortex motion that exactly matches a spatially uniform environmental geostrophic flow on an f plane are these terms zero. Geostrophy in the environment means that advection of environmental quantities by the environmental flow is small. One approach used in studies of vortex motion introduces a new velocity vector $\mathbf{v}' = \mathbf{v} - (\mathbf{c} - \tilde{\mathbf{c}})$. This change of variables replaces the explicit vortex accelerations on the right side of (2.12.1) with $(\mathbf{c} - \tilde{\mathbf{c}}) \cdot \nabla\,\mathbf{v}'$; see Willoughby (1992, 1994) for details. The separation of the total flow into vortex and environmental components is straightforward in synthesis of a theoretical model, but more difficult (and not necessarily unique) in analysis of observations (see Chapter 4.2 and 4.3).

Circular symmetry of tropical cyclones makes cylindrical coordinates a natural choice for representation of the motion in vortex-centered coordinates

$$\frac{\partial u}{\partial t}+\frac{v}{r}\frac{\partial u}{\partial \lambda}+u\frac{\partial u}{\partial r}+w\frac{\partial u}{\partial z}-v\left(\frac{v}{r}+f\right)+\frac{\partial \phi}{\partial r}=$$
$$-[\dot{c}_y+f(c_x-\tilde{c}_x)]\cos\lambda+[\dot{c}_x-f(c_y-\tilde{c}_y)]\sin\lambda+F_u, \qquad (2.13.1a)$$

$$\frac{\partial v}{\partial t}+\frac{v}{r}\frac{\partial v}{\partial \lambda}+u\left(\frac{\partial v}{\partial r}+\frac{v}{r}+f\right)+w\frac{\partial v}{\partial z}+\frac{1}{r}\frac{\partial \phi}{\partial \lambda}=$$
$$[\dot{c}_x-f(c_y-\tilde{c}_y)]\cos\lambda+[\dot{c}_y+f(c_x-\tilde{c}_x)]\sin\lambda+F_v, \qquad (2.13.1b)$$

$$\frac{\partial w}{\partial t}+\frac{v}{r}\frac{\partial w}{\partial \lambda}+u\frac{\partial w}{\partial r}+w\frac{\partial w}{\partial z}-g\frac{\theta-\theta_0}{\theta_0}+\frac{\partial \phi}{\partial z}=F_w, \qquad (2.13.2)$$

$$\frac{\partial u}{\partial r}+\frac{u}{r}+\frac{1}{r}\frac{\partial v}{\partial \lambda}+\frac{\partial w}{\partial z}-\frac{w}{H}=0, \qquad (2.13.3)$$

$$\frac{1}{\theta_0}\left[\frac{\partial \theta}{\partial t}+\frac{v}{r}\frac{\partial \theta}{\partial \lambda}+u\frac{\partial \theta}{\partial r}\right]+w\frac{N^2}{g}=-\frac{1}{\theta_0}\left[u\frac{\partial \tilde{\theta}}{\partial r}+\frac{v}{r}\frac{\partial \tilde{\theta}}{\partial \lambda}\right]+F_\theta, \qquad (2.13.4)$$

$$\frac{\partial q}{\partial t}+\frac{v}{r}\frac{\partial q}{\partial \lambda}+u\frac{\partial q}{\partial r}+w\frac{\partial q}{\partial z}=\frac{v}{r}\frac{\partial \tilde{q}}{\partial \lambda}+u\frac{\partial \tilde{q}}{\partial r}+E-C+F_q. \qquad (2.13.5)$$

Here, r is the distance from the axis of rotation, λ increases counterclockwise from north, and v has radial and tangential components u and v.

The dominance of the axisymmetric parts of the swirling wind and pressure anomaly in the TC core suggests the separation of the flow into axisymmetric and asymmetric parts might be a good strategy. Two techniques to accomplish the separation are available: small amplitude linearization and spectral expansion in azimuth. The first technique recognizes that v^*, the tangential velocity of the axisymmetric primary circulation, is much greater than either u_s and w_s, the radial and vertical velocities of the axisymmetric secondary circulation, or u_a, v_a, and w_a, the velocities of the asymmetric motions. The radially

symmetric geopotential and potential temperature anomalies, ϕ^* and θ^*, are also much greater than their asymmetric counterparts, ϕ_a and θ_a. The time scales of the changes in the axisymmetric motions are much slower than the orbital frequency of the swirling wind, which characterizes the temporal changes of the asymmetric motions (Shapiro and Willoughby 1982). The essence of the linearization is neglect of products between the smaller quantities to produce sets of linear equations for the symmetric and asymmetric motions. These equations are strictly valid only in the core. The second technique, spectral expansion, represents the motions as the sum of the axisymmetric flow and asymmetries that vary sinusoidally in azimuth. For each azimuthal wavenumber n, the asymmetric variables are the real parts of products between $e^{-in\lambda}$ and complex amplitudes that are functions of time, height, and radius. In addition to the actual asymmetries of the vortex, the motion and the environmental flow lend themselves to this "semispectral" representation. Because each Fourier component is linearly independent, the equations for its coefficients can be solved separately if wave-wave interactions are accounted for (Willoughby 1994). This technique retains advection of the asymmetric flow by the secondary circulation and both wave-wave interactions between the asymmetric components and wave-mean flow interactions with the axisymmetric vortex. The equations so derived are valid even in the outer vortex where the symmetric and asymmetric components have comparable strength.

2.5.2 Axisymmetric dynamics

The governing equations for the axisymmetric motions that emerge from the spectral decomposition are

$$\left\{\frac{\partial u_s}{\partial t}+u_s\frac{\partial u_s}{\partial r}+w_s\frac{\partial u_s}{\partial z}\right\}-v^*\left(\frac{v^*}{r}+f_0\right)+\frac{\partial \phi^*}{\partial r}=F_{u_s}. \tag{2.14.1a}$$

$$\frac{\partial v^*}{\partial t}+u_s\zeta^*+w_s\frac{\partial v^*}{\partial z}=M. \tag{2.14.1b}$$

$$\left\{\frac{\partial w_s}{\partial t}+u_s\frac{\partial w_s}{\partial r}+w_s\frac{\partial w_s}{\partial z}\right\}-g\frac{\theta^*}{\theta_0}+\frac{\partial \phi^*}{\partial z}=F_{w_s}. \tag{2.14.2}$$

$$\frac{\partial u_s}{\partial r}+\frac{u_s}{r}+\frac{\partial w_s}{\partial z}+\frac{w_s}{H}=0. \tag{2.14.3}$$

$$\frac{1}{\theta_0}\left[\frac{\partial \theta^*}{\partial t}+u_s\frac{\partial \theta^*}{\partial r}\right]+w_s\frac{N^2}{g}=Q. \tag{2.14.4}$$

$$\frac{\partial q_s}{\partial t}+u_s\frac{\partial q_s}{\partial r}+w_s\frac{\partial q_s}{\partial z}=E_s-C_s+F_{q_s}. \tag{2.14.5}$$

Here, $\zeta^* = \partial v^*/\partial r + v^*/r + f_0$ where $f = f_0 + \beta r \cos\lambda$, f_0 is the Coriolis parameter at the vortex center, and $\beta = \partial f/\partial y$. F_{us}, M, F_{ws} and Q include the axisymmetric part of the friction plus eddy flux convergences due to the asymmetric motions. The vortex motion and environmental flow interact primarily with wavenumber 1 and, to some extent, with wavenumbers ≥ 2. The only direct effects of the motion on the axisymmetric vortex occur through terms that arise from rectification in products such as $r\,\beta\cos\lambda \times (c_y - \tilde{c}_y)\cos\lambda$ or $(c_x - \tilde{c}_x)\cos\lambda$. In the TC core, the slow change of the axisymmetric flow with time, and the great strength of the primary circulation compared with the secondary circulation, imply that F_{us}, F_{ws}, and the terms in braces in (2.14.1a) and (2.14.2) are small. These are among the terms neglected in small amplitude linearization. Without them, the axisymmetric motions are in the gradient and hydrostatic balances

$$v^*\left(\frac{v^*}{r}+f_0\right)=\frac{\partial \phi^*}{\partial r}. \tag{2.15}$$

$$\frac{\partial \phi^*}{\partial z} = g\frac{\theta^*}{\theta_0}. \tag{2.16}$$

The axisymmetric thermal wind relation is derived by differentiation of (2.15) with respect to z and substitution from (2.16)

$$\left(\frac{2v^*}{r} + f_0\right)\frac{\partial v^*}{\partial z} = \xi^* S^* = \frac{g}{\theta_0}\frac{\partial \theta^*}{\partial r}, \tag{2.17}$$

where ξ^* is the inertia parameter of the swirling flow and S^* is its vertical shear.

Following Eliassen (1951), it is possible to use the balance relations to deduce the secondary circulation from the distribution of heat and momentum sources. Since the secondary circulation mass flow in the r-z plane is nondivergent, it may be represented with a streamfunction such that

$$\frac{\partial \psi_s}{\partial r} = r\rho_0 w_s, \qquad \frac{\partial \psi_s}{\partial z} = -r\rho_0 u_s. \tag{2.18}$$

The temporal changes may be eliminated between $\partial/\partial z$ of ξ^* times the tangential momentum equation (2.14.1b) and $\partial/\partial r$ of the thermodynamic energy (2.14.4) and substitution from (2.17) and (2.18) to produce a diagnostic (Eliassen) equation

$$\frac{\partial}{\partial z}\left(\frac{\zeta^*\xi^*}{r\rho_0}\frac{\partial \psi_s}{\partial z} - \frac{\xi^* S^*}{r\rho_0}\frac{\partial \psi_s}{\partial r}\right) + \frac{\partial}{\partial r}\left(\frac{N^2}{r\rho_0}\frac{\partial \psi_s}{\partial r} - \frac{\xi^* S^*}{r\rho_0}\frac{\partial \psi_s}{\partial z}\right) = -\frac{\partial(\xi^* M)}{\partial z} + \frac{\partial Q}{\partial r}. \tag{2.19}$$

Given the structure of the vortex and the distribution of heating and momentum sources, solution of this generalized Poisson equation yields the secondary circulation. Substitution of u_s and w_s into the tangential momentum equation (2.14.1b) allows calculation of $\partial v^*/\partial t$ to march the solution forward in a prognostic model (*e. g.*, Ooyama 1969; Sundqvist 1970a,b).

As discussed in Chapter 2.2, three parameters: static thermodynamic stability, N^2; inertial stability, $I^2 = \zeta^* \xi^* = r^{-3}\partial L^2/\partial r$; and baroclinicity, $B^2 = \xi^* S^* = r^{-3}\partial L^2/\partial z$; determine the character of the secondary circulation as described by (2.19), where $L = vr + f_0 r^2/2$ is the absolute angular momentum. As shown in Fig. 2.3, isolated sources of heat and momentum induce secondary circulations in an inhomogeneous vortex. Since the right side of (2.19) contains derivatives of L and Q, the streamfunction field due to an isolated patch of forcing is a dipole, i.e., two adjacent counterrotating elliptical gyres with flow between them passing through the source. For a heat source, the dipole axis that joins the foci of the ellipses is nearly horizontal. An updraft passes through the source and is flanked by compensating descent on either side. For a cyclonic momentum source, the dipole axis is nearly vertical with radial outflow passing through the source and compensating inflow above and below.

The spatial scales of the gyres are determined by the local Rossby radius of deformation, which is proportional to (N/I). Thus, variations of N^2, I^2, and B^2 distort the streamfunction patterns. When $N^2 > I^2$, forcing can overcome "inertia forces" more readily than buoyancy forces, so that the motions are primarily horizontal, and the streamfunction assumes a pattern of radially-elongated gyres. When $I^2 > N^2$, forcing can overcome buoyancy forces more readily than inertia forces so that the motions are primarily vertical, and the streamfunction pattern takes the form of vertically-elongated gyres. Heating adds buoyancy, but does not change angular momentum. A momentum source does not change

buoyancy. Thus, the updraft through a heat source in a baroclinic vortex tilts away from the vertical to follow surfaces of constant angular momentum, and the outflow through a momentum source inclines from the horizontal to follow surfaces of constant potential temperature.

2.5.3 Asymmetric dynamics

The linear governing equations for the asymmetric motions are

$$\frac{\partial u_a}{\partial t} + \frac{v^*}{r}\frac{\partial u_a}{\partial \lambda} - v_a\zeta^* + \frac{\partial \phi_a}{\partial r} = \mathcal{F}_{u_a}, \tag{2.20.1a}$$

$$\frac{\partial v_a}{\partial t} + \frac{v^*}{r}\frac{\partial v_a}{\partial \lambda} + u_a\zeta^* + \frac{\partial \phi_a}{\partial \lambda} = \mathcal{F}_{v_a}, \tag{2.20.1b}$$

$$\frac{\partial w_a}{\partial t} + \frac{v^*}{r}\frac{\partial w_a}{\partial \lambda} - g\frac{\theta_a}{\theta_0} + \frac{\partial \phi_a}{\partial z} = \mathcal{F}_{w_a}, \tag{2.20.2}$$

$$\frac{\partial u_a}{\partial r} + \frac{u_a}{r} + \frac{1}{r}\frac{\partial v_a}{\partial \lambda} + \frac{\partial w_a}{\partial z} - \frac{w_a}{H} = 0, \tag{2.20.3}$$

$$\frac{1}{\theta_0}\left[\frac{\partial \theta_a}{\partial t} + \frac{v^*}{r}\frac{\partial \theta_a}{\partial \lambda}\right] + \frac{1}{g}\left[u_a\zeta^* S^* + w_a N^2\right] = \frac{Q_a}{c_p T_0} + \mathcal{F}_{\theta_a}, \tag{2.20.4}$$

$$\frac{\partial q_a}{\partial t} + \frac{v^*}{r}\frac{\partial q_a}{\partial \lambda} + w_a\frac{\partial q_a}{\partial z} = E_a - C_a + \mathcal{F}_{q_a}. \tag{2.20.5}$$

Advection of the asymmetric components by the axisymmetric secondary circulation [terms analogous to those in brackets in (2.14.1a) and (2.14.2)] have been neglected, so that (2.20.1-2.20.5) are strictly valid only in the core. The *Fs* may include wave-wave interactions between the asymmetries and advection of environmental fields. An important term in the forcing on the right sides is $v^* r \beta \cos\lambda$ in F_{u_a}, which is the advection of planetary vorticity by the primary circulation. It forces the wavenumber 1 asymmetry directly--as do the actual and Coriolis accelerations of the vortex and the environmental pressure gradient. The interaction of $r\beta\cos\lambda$ with the mismatch between the vortex motion and the environmental flow forces wavenumber 2. If the environmental flow varies spatially, its relative vorticity gradient forces wavenumber 1, its deformation forces wavenumber 2, and its deformation gradient forces wavenumber 3 (Smith 1991; Willoughby 1994).

Internal gravity waves are an important class of disturbances described by (2.20.1-2.20.5). For a wavelike disturbance with tangential wavenumber n and frequency ω measured relative to the coordinate system, the Doppler-shifted frequency is $\Omega = \omega - nv^*/r$. If a wave packet is excited with some values of ω and n, these values will be conserved following the packet, but as the packet moves through the vortex, v^*, and hence Ω, will change. The quantities N^2 and I^2 play important roles in internal gravity wave dynamics as well as in forced circulations. Gravity waves are confined to a passband defined by $I^2 \leq \Omega^2 \leq N^2$. As Ω^2 is Doppler shifted to I^2, the horizontal wavelength becomes much greater than the vertical wavelength and the group velocity is directed horizontally. As Ω^2 is Doppler shifted to N^2, the horizontal wavelength becomes much less than the vertical wavelength and the group velocity is directed vertically. Near the ends of the passband at N^2 or I^2, the magnitude of the group velocity approaches zero. Gravity waves that propagate horizontally into sufficiently different swirling flow for their frequency to be Doppler shifted to the Brunt-Vaisala frequency experience critical radius absorption, a process

analogous to critical layer absorption either at zero frequency or I for their vertically propagating counterparts (Willoughby 1977).

2.6 SUMMARY

Tropical cyclones are warm-core, circular vortices maintained by convective release of latent heat extracted from the underlying sea. The azimuthally-averaged swirling wind is in gradient balance with the low pressure anomaly near the center. This swirling flow is cyclonic at low levels and near the center, but becomes anticyclonic near the tropopause level beyond 200 km from the center. A diabatically forced secondary circulation with a nearly isothermal near-surface inflow, saturated ascent around the center, and outflow near tropopause level, conveys (primarily latent) heat and momentum into the cyclone core. The secondary circulation is much weaker than the primary circulation except in the anticyclonic outflow, where the vortex is also much more asymmetric. The asymmetries near the tropopause converge angular momentum into the vortex from large radius and may be a key mechanism for environmental control of intensity and outer circulation strength. The most common mode of intensification involves contracting rings of convection organized by frictional convergence beneath local maxima of the swirling wind. In intense tropical cyclones, competition between multiple convective rings may lead to intensity fluctuations. Crucial unanswered questions lie in the sea's control of the potential intensity and vortex interactions with the synoptic-scale atmospheric environment that modulate the intensity within the envelope defined by oceanographic conditions.

REFERENCES

Abdullah, A. J., 1966: The spiral bands of a hurricane: A possible dynamic explanation. *J. Atmos. Sci.*, **23**, 367-375.

Allen, E. S., 1976: *A Wind to Shake the World.* Little-Brown and Co., Boston, 370 pp.

Andrews, D. G., and M. E. McIntyre, 1976: Planetary waves in horizontal and vertical shear: The generalized Eliassen-Palm relation and the mean zonal acceleration. *J. Atmos. Sci.*, **33**, 2031-2048.

Andrews, D. G., and M. E. McIntyre, 1978: Generalized Eliassen-Palm and Charney-Drazin theorems for waves on axisymmetric flows in compressible atmospheres. *J. Atmos. Sci.*, **35**, 175-185.

Anthes, R. A., and S. W. Chang, 1978: Response of the hurricane boundary-layer to changes of sea-surface temperature in a numerical model. *J. Atmos. Sci.*, **35**, 1240-1255.

Atkinson, G. D., and C. R. Holliday, 1977: Tropical cyclone minimum sea level pressure/maximum sustained wind relationship for the western North Pacific. *Mon. Wea. Rev.*, **105**, 421-427.

Atlas, D., K. R. Hardy, R. Wexler, and R. J. Boucher, 1963: The origin of hurricane spiral bands. *Geofis. Int.*, **3**, 123-132.

Barnes, G. M., E. J. Zipser, D. P. Jorgensen, and F. D. Marks, Jr., 1983: Mesoscale and convective scale structure of a hurricane rainband. *J. Atmos. Sci.*, **40**, 2125-2137.

Beer, T., and L. Giannini, 1980: Tropical cyclone cloudbands. *J. Atmos. Sci.*, **37**, 1511-1520.

Bergeron, T., 1954: The problem of tropical cyclones. *Quart. J. Roy. Meteor. Soc.*, **80**, 131-164.

Black, M. L., 1993: Comparisons of tropical cyclone intensity with eyewall vertical velocities. *Preprints, 20th Conf. Hurr. Trop. Meteor.*, Amer. Meteor. Soc., Boston, MA 02108, 520-523.

Black, M. L., and H. E. Willoughby, 1992: The concentric eyewall cycle of Hurricane Gilbert. *Mon. Wea. Rev.*, **120**, 947-957.

Black, P. G., 1983: Tropical storm structure as revealed by stereoscopic photographs from Skylab. *Adv. Space Res.*, **2**, 115-124.

Black, P. G., and R. A. Anthes, 1971: On the asymmetric structure of the tropical cyclone outflow layer. *J. Atmos. Sci.*, **28**, 1348-1366.

Black, P. G., and F. D. Marks, 1991: The structure of an eyewall meso-vortex in hurricane Hugo (1989). *Preprints, 19th Conf. Hurr. Trop. Meteor.*, Amer. Meteor. Soc., Boston, MA 02108, 579-582.

Black, R. A., and J. Hallett, 1986: Observations of the distribution of ice in hurricanes. *J. Atmos. Sci.*, **43**, 802-822.

Bluestein, H. B., and D. S. Hazen, 1989: Doppler-radar analysis of a tropical cyclone over land: Hurricane Alicia (1983) in Oklahoma. *Mon. Wea. Rev.*, **117**, 2594-2611.

Bosart, L. F., and F. H. Carr, 1978: A case study of excessive rainfall centered around Wellsville, New York, 20-21 June 1972. *Mon. Wea. Rev.*, **106**, 348-362.

Bosart, L. F., and D. B. Dean, 1991: The Agnes rainstorm of June 1972: Surface feature evolution culminating in inland storm redevelopment. *Wea. Forecasting*, **6**, 515-537.

Boyd, J. P., 1976: The noninteraction of waves with the zonally averaged flow on a spherical earth and the interrelationships of eddy fluxes of energy, heat and momentum. *J. Atmos. Sci.*, **33**, 2285-2291.

Brand, S., 1972: Very large and very small typhoons of the western North Pacific Ocean. *J. Meteor. Soc. Japan*, **50**, 332-341.

Brand, S., and J. W. Blelloch, 1973: Changes in the characteristics of typhoons crossing the Philippines. *J. Appl. Meteor.*, **12**, 104-109.

Brand, S., and J. W. Blelloch, 1974: Changes in the characteristics of typhoons crossing the island of Taiwan. *Mon. Wea. Rev.*, **102**, 708-713.
Brand, S., and C. P. Guard, 1979: An observational study of extratropical storms that evolved from tropical cyclones in the western North Pacific. *J. Meteor. Soc. Japan*, **57**, 479-482.
Burpee, R. W., and M. L. Black, 1989: Temporal and spatial variation of rainfall near the centers of two tropical cyclones. *Mon. Wea. Rev.*, **117**, 2208-2218.
Carr, L. E., and R. T. Williams, 1989: Barotropic vortex stability to perturbations from axisymmetry. *J. Atmos. Sci.*, **46**, 3177-3191.
Case, R. A., 1986: Atlantic hurricane season of 1985. *Mon. Wea. Rev.*, **114**, 1390-1405.
Case, R. A., and H. P. Gerrish, 1984: Atlantic hurricane season of 1983. *Mon. Wea. Rev.*, **112**, 1083-1092.
Challa, M., and R. L. Pfeffer, 1990: Formation of Atlantic hurricanes from cloud clusters and depressions. *J. Atmos. Sci.*, **47**, 909-927.
Clark, G. B., 1983: Atlantic hurricane season of 1982. *Mon. Wea. Rev.*, **111**, 1071-1079.
DeMaria, M., J.-J. Baik, and J. Kaplan, 1993: Upper-level angular momentum fluxes and tropical cyclone intensity change. *J. Atmos. Sci.*, **50**, 1133-1147.
DeMaria, M., and J. Kaplan, 1994: Sea surface temperature and the maximum intensity of Atlantic tropical cyclones. *J. Climate*, **7**, 1324-1334.
Deppermann, C. E., 1946: Is there a ring of violent upward convection in hurricanes and typhoons? *Bull. Amer. Meteor. Soc.*, **27**, 6-8.
DiMego, G. J., and L. F. Bosart, 1982a: The transformation of Tropical Storm Agnes into an extratropical cyclone. Part I: The observed fields and vertical motion computations. *Mon. Wea. Rev.*, **110**, 385-411.
DiMego, G. J., and L. F. Bosart, 1982b: The transformation of Tropical Storm Agnes into an extratropical cyclone. Part II: Moisture, vorticity and kinetic energy budgets. *Mon. Wea. Rev.*, **110**, 412-433.
Durst, C. S., and R. C. Sutcliffe, 1938: The importance of vertical motion in the development of tropical revolving storms. *Quart. J. Roy. Meteor. Soc.*, **64**, 75-84.
Dvorak, V. F., 1975: Tropical cyclone intensity analysis and forecasting from satellite imagery. *Mon. Wea. Rev.*, **103**, 420-430.
Dvorak, V. F., 1984: Tropical cyclone intensity analysis using satellite data. NOAA Tech. Rep. NESDIS 11, U. S. Department of Commerce, Washington, D.C. 20233, 47 pp.
Eliassen, A., 1951: Slow thermally or frictionally controlled meridional circulation in a circular vortex. *Astrophys. Norv.*, **5**, 19-60.
Eliassen, A., 1971: On the Ekman layer of a circular vortex. *J. Meteor. Soc. Japan*, **49**, 784-789.
Emanuel, K. A., 1984: A note on the stability of columnar vortices. *J. Fluid Mech.*, **145**, 235-238.
Emanuel, K. A., 1986: An air-sea interaction theory for tropical cyclones. Part I: Steady-state maintenance. *J. Atmos. Sci.*, **43**, 585-604.
Emanuel, K. A., 1988: The maximum intensity of hurricanes. *J. Atmos. Sci.*, **45**, 1143-1155.
Evans, J. L., 1993: Sensitivity of tropical cyclones to sea surface temperature. *J. Climate*, **6**, 1133-1140.
Fairall, C. W., J. D. Kepert, and G. J. Holland, 1995: The effect of sea spray on surface energy transports over the ocean. *J. Atmos. Sci.*, **52**, (submitted).
Fiorino, M., and R. L. Elsberry, 1989: Some aspects of vortex structure related to tropical cyclone motion. *J. Atmos. Sci.*, **46**, 975-990.
Fletcher, R. D., 1955: Computation of maximum surface winds in hurricanes. *Bull. Amer. Meteor. Soc.*, **36**, 247-250.
Frank, W. M., 1977a: The structure and energetics of the tropical cyclone. I: Storm structure. *Mon. Wea. Rev.*, **105**, 1119-1135.
Frank, W. M., 1977b: The structure and energetics of the tropical cyclone. II: Dynamics and energetics. *Mon. Wea. Rev.*, **105**, 1136-1150.
Frank, W. M., 1977c: Convective fluxes in tropical cyclones. *Mon. Wea. Rev.*, **105**, 1554-1568.
Frank, W. M., 1984: A composite analysis of the core of a mature hurricane. *Mon. Wea. Rev.*, **112**, 2401-2420.
Fujita, T. T., 1993: Wind fields of Andrew, Omar, and Iniki. *Preprints, 20th Conf. Hurr. Trop. Meteor.*, Amer. Meteor. Soc., Boston, MA 02108, 46-49.
Gentry, R. C., T. T. Fujita, and R. C. Sheets, 1970: Aircraft, spacecraft, and radar observations of Hurricane Gladys, 1968. *J. Appl. Meteor.*, **9**, 837-850.
Gray, W. M., 1968: Global view of the origin of tropical disturbances and storms. *Mon. Wea. Rev.*, **96**, 669-700.
Gray, W. M., 1991: Comment on "Gradient balance in tropical cyclones." *J. Atmos. Sci.*, **48**, 1201-1208.
Gray, W. M., and D. J. Shea, 1973: The hurricane's inner core region. II. Thermal stability and dynamic characteristics. *J. Atmos. Sci.*, **30**, 1565-1576.
Guinn, T. A., and W. H. Schubert, 1993a: Polygonal eyewalls in hurricanes. *Preprints, 20th Conf. Hurr. Trop. Meteor.*, Amer. Meteor. Soc., Boston, MA 02108, J30-J31.
Guinn, T. A., and W. H. Schubert, 1993b: Hurricane spiral bands. *J. Atmos. Sci.*, **50**, 3380-3403.
Haurwitz, B., 1935: The height of tropical cyclones and the eye of the storm. *Mon. Wea. Rev.*, **63**, 45-49.
Hawkins, H. F., 1983: Hurricane Allen and island obstacles. *J. Atmos. Sci.*, **40**, 1360-1361.
Hawkins, H. F., and D. T. Rubsam, 1968: Hurricane Hilda, 1964. II. Structure and budgets of the hurricane on October 1 1964. *Mon. Wea. Rev.*, **96**, 617-636.
Hawkins, H. F., and S. M. Imbembo, 1976: The structure of a small intense hurricane - Inez, 1966. *Mon. Wea. Rev.*, **104**, 418-442.
Hiser, H. W., and W. L. Freseman, 1959: *Radar Meteorology*. 2nd Ed., University of Miami, Coral Gables, FL 33143, 205-207.
Holland, G. J., 1980: An analytic model of the wind and pressure profiles in hurricanes. *Mon. Wea. Rev.*, **108**, 1212-1218.
Holland, G. J., 1983a: Angular momentum transports in tropical cyclones. *Quart. J. Roy. Meteor. Soc.*, **109**, 187-209.

Holland, G. J., 1983b: Tropical cyclone motion: Environmental interaction plus a beta effect. *J. Atmos. Sci.*, **40**, 328-382.
Holland, G. J., 1984: On the climatology and structure of tropical cyclones in the Australian Southwest Pacific Region. II. Hurricanes. *Aus. Meteor. Mag.*, **32**, 17-31.
Holland, G. J., and R. T. Merrill, 1984: On the dynamics of tropical cyclone structural changes. *Quart. J. Roy. Meteor. Soc.*, **110**, 723-745.
Holliday, C. R., 1977: Double intensification of Typhoon Gloria, 1974. *Mon. Wea. Rev.*, **105**, 523-528.
Holliday, C. R., and A. H. Thompson, 1979: Climatological characteristics of rapidly intensifying typhoons. *Mon. Wea. Rev.*, **107**, 1022-1034.
Holton, J. R., 1992: *An Introduction to Dynamic Meteorology*. 3rd Ed., Academic Press, pp. 253-254.
Hoose, H. M., and J. A. Colon, 1970: Some aspects of the radar structure of Hurricane Beulah on September 9, 1967. *Mon. Wea. Rev.*, **98**, 529-533.
Houze, R. A., and A. K. Betts, 1981: Convection in GATE. *Rev. Geophys. Space Phys.*, **19**, 541-576.
Hubert, L. F., 1955: Frictional filling of hurricanes. *Bull. Amer. Meteor. Soc.*, **36**, 440-445.
Hughes, L. A., 1952: On the low-level wind structure of tropical storms. *J. Meteor.*, **9**, 422-428.
Ishihara, M., Z. Yanagisawa, H. Sakakibara, K. Matsuura, and J. Aoyagi, 1986: Structure of a typhoon rainband observed by two Doppler radars. *J. Meteor. Soc. Japan*, **64**, 923-938.
Jordan, C. L., 1958: The thermal structure of tropical cyclones. *Geophysica*, **6**, 281-297.
Jordan, C. L., 1961: Marked changes in the characteristics of the eye of intense typhoons between the deepening and filling stages. *J. Meteor.*, **18**, 779-789.
Jordan, C. L., 1966: Surface pressure variations at coastal stations during the period of irregular motion of Hurricane Carla of 1961. *Mon. Wea. Rev.*, **94**, 454-458.
Jordan, C. L., and E. S. Jordan, 1954: On the mean thermal structure of tropical cyclones. *J. Meteor.*, **11**, 440-448.
Jordan, C. L., D. A. Hurt, and C. A. Lowrey, 1960: On the structure of Hurricane Daisy on 27 August 1958. *J. Meteor.*, **17**, 337-348.
Jordan, E. S., 1952: An observational study of the upper wind circulation around tropical storms. *J. Meteor.*, **9**, 340-346.
Jorgensen, D. P., 1984a: Mesoscale and convective-scale characteristics of mature hurricanes. Part I: General observations by research aircraft. *J. Atmos. Sci.*, **41**, 1268-1285.
Jorgensen, D. P., 1984b: Mesoscale and convective-scale characteristics of mature hurricanes. Part II: Inner core structure of Hurricane Allen (1980). *J. Atmos. Sci.*, **41**, 1287-1311.
Jorgensen, D. P., and P. T. Willis, 1982: A Z-R relationship for hurricanes. *J. Appl. Meteor.*, **21**, 356-366.
Jorgensen, D. P., E. J. Zipser, and M. A. LeMone, 1985: Vertical motions in intense hurricanes. *J. Atmos. Sci.*, **42**, 839-856.
Koteswaram, P., 1967: On the structure of hurricanes in the upper troposphere and lower stratosphere. *Mon. Wea. Rev.*, **95**, 541-564.
Kepert, J. D., 1995: Heat and moisture budgets of the tropical cyclone subcloud layer. *J. Atmos. Sci.*, **52**, (submitted)
Korolev, V. S., S. A. Petrichenko, and V. D. Pudov, 1990: Heat and moisture exchange between the ocean and atmosphere in Tropical Storms Tess and Skip. *Soviet Meteor. Hydrol.*, **3**, 92-94 (English translation).
Kuo, H. L., 1959: Dynamics of convective vortices and eye formation. *The Atmosphere and Sea in Motion*, B. Bolin, Ed., Rockefeller Institute Press, 413-424.
Kurihara, Y., 1976: On the development of spiral rainbands in a tropical cyclone. *J. Atmos. Sci.*, **33**, 940-958.
La Seur, N. E., and H. F. Hawkins, 1963: An analysis of Hurricane Cleo (1958) based on data from research reconnaissance aircraft. *Mon. Wea. Rev.*, **91**, 694-709.
Lee, C.-S., 1984: The bulk effect of cumulus momentum transports in tropical cyclones. *J. Atmos. Sci.*, **41**, 590-603.
Leslie, L. M., and R. K. Smith, 1970: The surface boundary layer of a hurricane II. *Tellus*, **22**, 288-297.
Lewis, B. M., and H. F. Hawkins, 1982: Polygonal eyewalls and rainbands in hurricanes. *Bull. Amer. Meteor. Soc.*, **63**, 1294-1300.
Ligda, M. G. H., 1955a: Analysis of motion of small precipitation areas and bands in the hurricane August 23-28, 1949. Tech. Note No. 3, Dept. of Meteor., Mass. Instit. Tech., 36 pp.
Ligda, M. G. H., 1955b: Hurricane squall lines. *Bull. Amer. Meteor. Soc.*, **36**, 340-342.
MacDonald, N. J., 1968: The evidence for the existence of Rossby-like waves in the hurricane vortex. *Tellus*, **20**, 138-146.
Malkus, J. S., 1958: On the structure and maintenance of the mature hurricane eye. *J. Meteor.*, **15**, 337-349.
Malkus, J. S., 1959: Recent developments in studies of penetrative convection and an application to hurricane cumulonimbus towers. *Cumulus Dynamics*, C. E. Anderson, Ed., Pergamon Press, 65-83.
Malkus, J. S., C. Ronne, and M. Chaffee, 1961: Cloud patterns in Hurricane Daisy, 1958. *Tellus*, **13**, 8-30.
Malkus, J. S., and H. Riehl, 1960: On the dynamics and energy transformations in steady--state hurricanes. *Tellus*, **12**, 1-20.
Malkus, J. S., and R. H. Simpson, 1964: Note on the potentialities of cumulonimbus and hurricane seeding experiments. *J. Appl. Meteor.*, **3**, 470-475.
Marks, F. D., 1985: Evolution of the structure of precipitation in Hurricane Allen (1980). *Mon. Wea. Rev.*, **113**, 909-930.
Marks, F. D., and R. A. Houze, 1984: Airborne Doppler radar observations in Hurricane Debby. *Bull. Amer. Meteor. Soc.*, **65**, 569-582.
Marks, F. D., and R. A. Houze, 1987: Inner core structure of Hurricane Alicia from Doppler radar observations. *J. Atmos. Sci.*, **44**, 1296-1317.
Maynard, R. H., 1945: Radar and weather. *J. Meteor.*, **2**, 214-226.

McBride, J. L., and T. D. Keenan, 1982: Climatology of tropical cyclone genesis in the Australian region. *J. Climatol.*, **2**, 13-33.
Menard, R. D., and J. M. Fritsch, 1989: A mesoscale convective complex-generated inertially stable warm vortex. *Mon. Wea. Rev.*, **117**, 1237-1261.
Merrill, R. T., 1984: A comparison of large and small tropical cyclones. *Mon. Wea. Rev.*, **112**, 1408-1418.
Merrill, R. T., 1988a: Characteristics of the upper tropospheric environmental flow around hurricanes. *J. Atmos. Sci.*, **45**, 1665-1677.
Merrill, R. T., 1988b: Environmental influences on hurricane intensification. *J. Atmos. Sci.*, **45**, 1678-1687.
Miller, B. I., 1958: On the maximum intensity of hurricanes. *J. Meteor.*, **15**, 184-195.
Miller, B. I., 1964: A study of the filling of Hurricane Donna (1960) over land. *Mon. Wea. Rev.*, **92**, 389-406.
Molinari, J., and S. Skubis, 1985: Evolution of the surface wind field in an intensifying tropical cyclone. *J. Atmos. Sci.*, **42**, 2865-2879.
Molinari, J., and D. Vollaro, 1989: External influences on hurricane intensity: Part I. Outflow layer eddy angular momentum fluxes. *J. Atmos. Sci.*, **46**, 1093-1105.
Molinari, J., and D. Vollaro, 1990: External influences on hurricane intensity: Part II. Vertical structure and response of the hurricane vortex. *J. Atmos. Sci.*, **47**, 1902-1918.
Montgomery, M. T., and B. M. Farrell, 1993: Tropical cyclone formation. *J. Atmos. Sci.*, **50**, 285-310.
Moss, M. S., 1978: Low-level turbulence structure in the vicinity of a hurricane. *Mon. Wea. Rev.*, **106**, 841-849.
Moss, M. S., and S. L. Rosenthal, 1975: On the estimation of planetary boundary layer variables in mature hurricanes. *Mon. Wea. Rev.*, **103**, 980-988.
Moss, M. S., and F. J. Merceret, 1976: A note on several low-layer features of Hurricane Eloise (1975). *Mon. Wea. Rev.*, **104**, 967-971.
Muramatsu, T., 1986: Trochoidal motion of the eye of Typhoon 8019. *J. Meteor. Soc. Japan*, **64**, 259-272.
Myers, V. A., 1957: Maximum hurricane winds. *Bull. Amer. Meteor. Soc.*, **38**, 227-228.
Neuman, S., and J. G. Boyd, 1962: Hurricane movement and variable location of high intensity spot in wall cloud radar echo. *Mon. Wea. Rev.*, **90**, 371-374.
Novlan, D. J., and W. M. Gray, 1974: Hurricane spawned tornadoes. *Mon. Wea. Rev.*, **102**, 476-488.
Ooyama, K. V., 1969: Numerical simulation of the life cycle of tropical cyclones. *J. Atmos. Sci.*, **26**, 3-40.
Ooyama, K. V., 1982: Conceptual evolution of the theory and modeling of the tropical cyclone. *J. Meteor. Soc. Japan*, **60**, 369-380.
Padya, M, 1975: Spatial variability and gustiness of cyclone winds: Gervaise, Mauritius, February 1975. *Aus. Meteor. Mag.*, **23**, 61-69.
Palmen, E., 1948: On the formation and structure of tropical hurricanes. *Geophysica*, **3**, 26-38.
Palmen, E., 1956: Formation and development of tropical cyclones. *Proc., Trop. Cyclone Symp. Brisbane,* Australian Bureau of Meteorology, Melbourne, Australia 3001, 213-231.
Palmen, E., 1958: Vertical circulation and release of kinetic energy during the development of Hurricane Hazel into an extratropical storm. *Tellus*, **10**, 1-23.
Palmen, E., and C. W. Newton, 1969: *Atmospheric Circulation Systems*. Academic Press, New York, 603 pp.
Parrish, J. R., R. W. Burpee, F. D. Marks, Jr., and R. Grebe, 1982: Rainfall patterns observed by digitized radar during landfall of Hurricane Frederic (1979). *Mon. Wea. Rev.*, **110**, 1933-1944.
Pasch, R. J., and L. A. Avila, 1992: Atlantic hurricane season of 1991. *Mon. Wea. Rev.*, **120**, 2671-2687.
Pearlroth, I., 1962: Relationship of central pressure of hurricane Esther (1961) and the sea surface temperature field. *Tellus*, **14**, 403-408.
Pearlroth, I., 1967: Hurricane behavior as related to oceanographic environmental conditions. *Tellus*, **19**, 258-268.
Peng, M. S., and R. T. Williams, 1991: Stability analysis of barotropic vortices. *Geophys. Astrophys. Fluid Dyn.*, **58**, 263-283.
Pfeffer, R. L., 1958: Concerning the mechanics of hurricanes. *J. Meteor.*, **15**, 113-120.
Pfeffer, R. L., and M. Challa, 1992: The role of environmental asymmetries in Atlantic hurricane formation. *J. Atmos. Sci.*, **49**, 1051-1059.
Powell, M. D., 1982: The transition of the Hurricane Frederic boundary-layer wind field from the open Gulf of Mexico to landfall. *Mon. Wea. Rev.*, **110**, 1912-1932.
Powell, M. D., 1987: Changes in the low-level kinematic and thermodynamic structure of Hurricane Alicia (1983) at landfall. *Mon. Wea. Rev.*, **115**, 75-99.
Powell, M. D., 1990a: Boundary-layer structure and dynamics in outer hurricane rainbands. Part I: Mesoscale rainfall and kinematic structure. *Mon. Wea. Rev.*, **118**, 891-917.
Powell, M. D., 1990b: Boundary-layer structure and dynamics in outer hurricane rainbands. Part II: Downdraft modification and mixed layer recovery. *Mon. Wea. Rev.*, **118**, 918-938.
Powell, M. D., and P. G. Black, 1990: Meteorological aspects of Hurricane Hugo's landfall in the Carolinas. *Shore and Beach*, **58**(4), 3-14.
Ramage, C. S., 1974: The typhoons of October 1970 in the South China Sea: Intensification, decay, and ocean interaction. *J. Appl. Meteor.*, **13**, 739-751.
Ramanathan, V., and W. Collins, 1991: Thermodynamic regulation of ocean warming by cirrus clouds deduced from observations of the 1987 El Nino. *Nature*, **351**, 27-32.
Riehl, H., 1948: A radiosonde observation in the eye of a hurricane. *Quart. J. Roy. Meteor. Soc.*, **74**, 194-196.
Riehl, H., 1963: Some relations between wind and thermal structure of steady state hurricanes. *J. Atmos. Sci.*, **20**, 276-287.
Riehl, H., 1981: Vertical exchange of momentum and energy in the subcloud layer of Australian Hurricane Kerry (1979). *Tellus*, **33**, 105-108.
Riehl, H., and J. S. Malkus, 1961: Some aspects of Hurricane Daisy, 1958. *Tellus*, **13**, 181-213.
Rodgers, E. B., J.-J. Baik, and H. F. Pierce, 1994: Environmental influence on tropical cyclone precipitation. *J. Appl. Meteor.*, **33**, 129-139.

Roll, H. U., 1965: *Physics of the Marine Atmosphere*. Academic Press, 251-252.
Rotunno, R., and K. A. Emanuel, 1987: An air-sea interaction theory for tropical cyclones. Part II. Evolutionary study using a nonhydrostatic axisymmetric numerical model. *J. Atmos. Sci.*, **44**, 542-561.
Sadler, J. C., 1976: A role of the tropical upper tropospheric trough in early season typhoon development. *Mon. Wea. Rev.*, **104**, 1266-1278.
Sawyer, J. H., 1947: Notes on the theory of tropical cyclones. *Quart. J. Roy. Meteor. Soc.*, **73**, 101-126.
Schloemer, R. W., 1954: Analysis and synthesis of hurricane wind patterns over Lake Okechobee, Florida. Hydromet. Report No. 31, 39 pp. [U.S. Govt. Printing Office No. C30.70:31].
Schubert, W. H., and J. J. Hack, 1982: Inertial stability and tropical cyclone development. *J. Atmos. Sci.*, **39**, 1687-1697.
Schwartz, F. K., 1970: The unprecedented rains in Virginia associated with the remnants of Hurricane Camille. *Mon. Wea. Rev.*, **98**, 851-859.
Sekioka, M., 1970: On the behavior of cloud patterns as seen on satellite photographs in the transformation of a typhoon into an extratropical cyclone. *J. Meteor. Soc. Japan*, **48**, 224-232.
Senn, H. V., and H. W. Hiser, 1959: On the origin of hurricane spiral rain bands. *J. Meteor.*, **16**, 419-426.
Shapiro, L. J., 1983: The asymmetric boundary layer under a translating hurricane. *J. Atmos. Sci.*, **40**, 1984-1998.
Shapiro, L. J., and H. E. Willoughby, 1982: The response of balanced hurricanes to local sources of heat and momentum. *J. Atmos. Sci.*, **39**, 378-394.
Shapiro, L. J., and M. T. Montgomery, 1993: A three-dimensional balance theory for rapidly rotating vortices. *J. Atmos. Sci.*, **50**, 3322-3335.
Shaw, W. N., 1922: The birth and death of cyclones. Reprinted in *Selected Meteorological Papers of Sir Napier Shaw*, Macdonald, London, 1955, 207-221.
Shay, L. K., P. G. Black, A. J. Mariano, J. D. Hawkins, and R. L. Elsberry, 1992: Upper ocean response to Hurricane Gilbert. *J. Geophys. Res.*, **97**, 20227-20248.
Shea, D. J., and W. M. Gray, 1973: The hurricane's inner core region. I. Symmetric and asymmetric structure. *J. Atmos. Sci.*, **30**, 1544-1564.
Sherman, L., 1956: On the wind asymmetry of hurricanes. *J. Meteor.*, **13**, 500-503.
Simpson, R. H., and H. Riehl, 1958: Mid-tropospheric ventilation as a constraint on hurricane development and maintenance. *Proc., Tech. Conf. Hurr.*, Amer. Meteor. Soc., Boston, MA 02108, D4.1-D4.10.
Smith, R. K., 1968: The surface boundary layer of a hurricane. *Tellus*, **20**, 473-484.
Smith, R. K., 1981: The cyclostrophic adjustment of vortices with application to tropical cyclone modification. *J. Atmos. Sci.*, **38**, 2021-2030.
Smith, R. K., 1991: An analytic theory of tropical cyclone motion in a barotropic shear flow. *Quart. J. Roy. Meteor. Soc.*, **117**, 685-714.
Sundqvist, H., 1970a: Numerical simulation of the development of tropical cyclones with a ten-level model. Part I. *Tellus*, **22**, 359-390.
Sundqvist, H., 1970b: Numerical simulation of the development of tropical cyclones with a ten-level model. Part II. *Tellus*, **22**, 504-510.
Tuleya, R. E., 1994: Tropical storm development and decay: Sensitivity to surface boundary conditions. *Mon. Wea. Rev.*, **122**, 291-304.
Wakimoto, R. M., and P. G. Black, 1994: Damage survey of Hurricane Andrew and its relationship to the eyewall. *Bull. Amer. Meteor. Soc.*, **75**, 189-200.
Weatherford, C. L., and W. M. Gray, 1988a: Typhoon structure as revealed by aircraft reconnaissance. Part I: Data analysis and climatology. *Mon.Wea. Rev.*, **116**, 1032-1043.
Weatherford, C. L., and W. M. Gray, 1988b: Typhoon structure as revealed by aircraft reconnaissance. Part II: Structural variability. *Mon. Wea. Rev.*, **116**, 1044-1056.
Weber, H. C., and R. K. Smith, 1993: The stability of barotropic vortices: Implications for tropical cyclone motion. *Geophys. Astrophys. Fluid Dyn.*, **70**, 1-30.
Wexler, H., 1947: Structure of hurricanes as determined by radar. *Ann. N. Y. Acad. Sci.*, **48**, 821-844.
Willoughby, H. E., 1977: Inertia-buoyancy waves in hurricanes. *J. Atmos. Sci.*, **34**, 1028-1039.
Willoughby, H. E., 1978: A possible mechanism for the formation of hurricane rainbands. *J. Atmos. Sci.*, **35**, 838-848.
Willoughby, H. E., 1979: Forced secondary circulations in hurricanes. *J. Geophys. Res.*, **84**, 3173-3183.
Willoughby, H. E., 1988: The dynamics of the tropical cyclone core. *Aus. Meteor. Mag.*, **36**, 183-191.
Willoughby, H. E., 1990a: Temporal changes in the primary circulation in tropical cyclones. *J. Atmos. Sci.*, **47**, 242-264.
Willoughby, H. E., 1990b: Gradient balance in tropical cyclones. *J. Atmos. Sci.*, **47**, 265-274.
Willoughby, H. E. 1990c: Linear normal modes of a shallow-water barotropic vortex. *J. Atmos. Sci.*, **47**, 2141-2148.
Willoughby, H. E., 1991: Reply (to W. M. Gray: "Comment on 'Gradient balance in tropical cyclones'"). *J. Atmos. Sci.*, **48**, 1209-1212.
Willoughby, H. E., 1992: Linear motion of a shallow-water barotropic vortex as an initial-value problem. *J. Atmos. Sci.*, **49**, 2015-2031.
Willoughby, H. E., 1994: Nonlinear motion of a shallow-water barotropic vortex. *J. Atmos. Sci.*, **51**, 3722-3744.
Willoughby, H. E., J. A. Clos, and M. G. Shoreibah, 1982: Concentric eye walls, secondary wind maxima, and the evolution of the hurricane vortex. *J. Atmos. Sci.*, **39**, 395-411.
Willoughby, H. E., F. D. Marks, and R. J. Feinberg, 1984: Stationary and moving convective bands in hurricanes. *J. Atmos. Sci.*, **41**, 3189-3211.
Willoughby, H. E., D. P. Jorgensen, R. A. Black, and S. L. Rosenthal, 1985: Project STORMFURY: A scientific chronicle 1962-1983. *Bull. Amer. Meteor. Soc.*, **66**, 505-514.

Willoughby, H. E., J. M. Masters, and C. W. Landsea, 1989: A record minimum pressure observed in Hurricane Gilbert. *Mon. Wea. Rev.*, **117**, 2824-2828.
Wood, F. B., and H. Wexler, 1945: A flight into the September, 1944 hurricane off Cape Henry, Virginia. *Bull. Amer. Meteor. Soc.*, **26**, 153-159.
Xu, Q., 1983: Unstable spiral inertial gravity waves in typhoons. *Sci. Sinica*, **26**, 70-80.
Yamamoto, R., 1963: A dynamical theory of spiral rain band in tropical cyclones. *Tellus*, **15**, 155-161.
Yeh, T.-C., and R. L. Elsberry, 1993: Interaction of typhoons with the Taiwan orography. Part I. Upstream track deflections. *Mon. Wea. Rev.*, **121**, 3193-3212.
Zehnder, J. A., 1993: The influence of large-scale topography on barotropic vortex motion. *J. Atmos. Sci.*, **50**, 2519-2532.